Title
The effects of mitochondrial stress on organismal health in C. elegans

Author
Henderson, Hope Rosalind

Publication Date
2019

Peer reviewed|Thesis/dissertation

The effects of mitochondrial stress on organismal health in *C. elegans*

By
Hope Rosalind Henderson

A dissertation submitted in partial satisfaction of the

requirements for the degree of

Doctor of Philosophy

in

Molecular and Cell Biology

in the

Graduate Division

of the

University of California, Berkeley

Committee in charge:

Professor Andrew Dillin
Dean Michael Botchan
Professor Abby Dernburg
Assistant Professor Michael Shapira

Spring 2019

Abstract

The effects of mitochondrial stress on organismal health in *C. elegans*
By
Hope Rosalind Henderson
Doctor of Philosophy in Molecular and Cell Biology
University of California, Berkeley
Professor Andrew Dillin, Chair

Mitochondria are an essential organelle, serving as a key site of energy production in metazoans. Animals have complex systems for monitoring the health and proteostasis of mitochondria, and activate multiple quality control mechanisms in response to dysfunction. Using the nematode *Caenorhabditis elegans*, we investigated mitochondrial health, dysfunction, and stress signaling in two different systems.

Dysfunction of mitochondrial DNA replication machinery is a common cause of mitochondrial diseases. The minimal mammalian replisome is made up of DNA polymerase gamma, replicative helicase Twinkle, and single-stranded DNA binding protein. Recently, a sequence homolog of Twinkle was uncovered in the nematode *C. elegans*. Here, we characterized this homolog, *twnk-1*, and report that while *twnk-1* does not appear function as the primary mitochondrial DNA replicative helicase in this species, as loss of *twnk-1* does not result in reduce mitochondrial DNA levels, or result in other expected mitochondrial dysfunctions such as reduced oxygen consumption rates, increased sensitivity to metabolic perturbations, or reduced muscle function. However, *twnk-1* mutants exhibit phenotypes associated with mitochondrial stress, including reduced fecundity, an activation of the mitochondrial unfolded protein response (UPR^{mt}), and mitochondrial fragmentation. Our results suggest that in *C. elegans*, *twnk-1* does not function as the mitochondrial DNA replicative helicase, but has an alternative function in regulating mitochondrial function.

In a second project, we focused on the UPR^{mt}, a transcriptional program initiated when mitochondrial proteostasis is challenged. Previous work from our lab shows that when mitochondrial health is challenged in neurons alone, they signal to distal tissues, activating the UPR^{mt} in the intestine. This causes hormesis as shown through extended lifespan. We found that when the UPR^{mt} component and chromatin modifier PHF8/*jmjd-1.2a* is overexpressed in a second neural cell type, astrocyte-like cephalic sheath glia, they signal the UPR^{mt} to distal tissues as well. We used two UPR^{mt} reporters to investigate this effect, and to dissect the details of the two branches of UPR^{mt} signaling. Glial UPR^{mt} induced hormesis as shown through extended lifespan, as well as resistance to the mitochondrial stressor paraquat. This work contributes to the growing field of glia biology and supports the hypothesis that glia are actively involved in information processing and signaling.

Table of Contents

Acknowledgements

To Dr. Andrew Dillin—thank you for giving me the opportunity and support to do this work. To Dr. Anu Soumaleinan—thank you for your mentorship with the Twinkle project. To my co-authors and collaborators Dr. Liliya Euro, Dr. Jenni Durieux, Dr. Raz Bar-Ziv, and Samira Monshietehadi —thank you for your fine work. To the many Dillin lab members throughout the years—thank you for your advice, help, and expertise. To Dr. Ryo Higuchi-Sanabria and Dr. Aaron Friedman—thank you for your friendship. To Jason Kelley—Danez Smith said it better than I can in his "acknowledgements".

I would like to dedicate this work to Dr. Selena Ellis, without whom I would not be here.

Chapter 1: Introduction

In my graduate work, I used *C. elegans* to model and investigate mitochondrial dysfunction and stress responses. As introduced here and detailed in chapter 3, in my first project, I investigated a putative mitochondrial DNA replisome protein, the helicase Twinkle, and characterized organismal response to knockdown and knockout of this protein, which is essential in other invertebrate and mammalian models. In my second project, detailed in chapter 4, I investigated the ability of glia cells are able to perceive mitochondrial stress and activate a hormetic response via cell non-autonomous signaling of the mitochondrial unfolded protein response.

1.1 Mitochondria, mitochondrial dysfunction, and quality control

Mitochondria are essential organelles, responsible for cellular energy production and the synthesis of metabolites in metazoa. They are the site of β-oxidation of fatty acids and oxidative phosphorylation, have essential roles in calcium homeostasis and apoptosis, and drive anabolic biosynthesis events that support cellular growth. Mitochondrial function is crucial to healthspan and lifespan. Aberrant mitochondrial function can trigger a wide range of metabolic consequences, and mitochondrial dysfunction is associated with numerous genetic and age-onset diseases (1).

Mitochondria evolved from archaeabacteria, and became obligate symbionts in many eukaryotic cells. They retain remnants of their evolutionary history; notably, a double membrane and their own circular genome (2). Over time, most genes from the original bacterial genome have either been transferred to the nuclear genome, or lost. In metazoans, mitochondria maintain a small genome (~15 kb), which contains 12-13 crucial genes encoding subunits of the multimeric electron transport chain (ETC) protein complexes, while the rest of the ETC proteins are encoded by the nuclear genome. Additionally, the mitochondrial genome contains the sequences to make mitochondrial tRNAs and rRNAs. All other mitochondrial proteins are transcribed from the nuclear genome, and then imported into the organelle by designated protein import mechanisms (3,4) in the outer mitochondrial membrane (OMM) and inner mitochondrial membrane (IMM).

The OMM is made of phospholipid bilayer studded with proteins involved in fission and fusion, lipid processing, and protein import. The IMM is also a phospholipid bilayer, and it contains protein import components, proteases, and crucially, houses all complexes of the electron transport chain (ETC) and ATP synthase. The inner-most compartment of the mitochondria, the matrix, contains enzymes for the TCA cycle and fatty acid metabolism, as well as machinery for mitochondrial DNA (mtDNA) replication, transcription, and translation machinery. The mtDNA nucleoid itself is also in the matrix, closely associated with the matrix-facing side of the IMM.

Mitochondrial function declines in normal aging. In aging in various model organisms, we see an increase in mtDNA deletions and mutations, and increased production of reactive oxygen species (ROS). There is decreased expression of nuclear-encoded mitochondrial genes, decreased oxygen consumption rate (OCR), and decreased production of ATP (5). Mitochondrial membrane potential decreases, presumably decreasing the capacity for protein import (6), which

is also speculated to cause an increase in protein mistargeting to subcellular locations during aging.

Mitochondria face several unique challenges to their maintaining their health in the cellular environment. First, because most mitochondrial proteins are transcribed from the nucleus and translated in the cytoplasm, the overwhelming majority of mitochondrial proteins must be imported into the organelle. This requires cytosolic chaperones, healthy OMM and IMM import complexes, high mitochondrial membrane potential, and faithful targeting to the correct organelle. Another challenge is that the vital mitochondrial protein complexes responsible for oxidative phosphorylation (OXPHOS) contain protein subunits encoded by both the nuclear and mitochondrial genomes. Expression of these subunits must be coordinated across the two genomes, and failure in this coordination leads to stoichiometric imbalances in the protein complexes which cause stress to the organelle. A third unique challenge is that oxidative phosphorylation creates reactive oxygen species (ROS) as a byproduct. ROS can harm the OXPHOS machinery, mtDNA, and other mitochondrial proteins and lipids.

Over the past several decades, research has increasingly suggested a causative link between mitochondrial dysfunction, aging, and late-onset disease. Aberrant mitochondrial function can trigger a wide range of metabolic consequences, and mitochondrial dysfunction is associated with numerous neurodegenerative diseases of aging. Hundreds of genetic variants in mitochondrial proteins have been associated with pathological changes in mitochondrial function, many of which manifest only later in life.

Cells orchestrate and coordinate a handful of known stress-response mechanisms that are induced by various mitochondrial perturbations caused by these and other challenges. Mitochondria are constantly undergoing fission and fusion events, which dilute the effects of damage in any individual organelle. In *C. elegans*, mitochondrial fragmentation—that is, the appearance hyperfused, oversized mitochondrial foci—is a stereotyped response to stress, presumably working to join together compromised organelles to get a full compliment of working machinery, proteins, and intact nucleoids (7,8). Another mechanism is autophagy of mitochondria (mitophagy), in which E3 ligase Parkin and kinase PINK1 work together to ubiquitinate the surface of damaged organelles, targeting them for degradation (9). Recently, there have been descriptions of mitochondrial-derived vesicles pinched off the organelle and bound for degradation (10,11). Apoptosis may be initiated is when the load of mitochondrial stress is insurmountable (12–14).

Our work focuses on the final known quality control mechanism: the mitochondrial unfolded protein response (UPR^{mt}), a protective transcriptional regulation program activated upon mitochondrial stress. In this response, mitochondria signal stress to the nucleus, which reduces global transcription, but increases transcription of mitochondrial protein chaperones and proteases to restore proteostasis in the organelle. Over the last decade, our and other labs have uncovered many of the key molecular players in this process. The initial signal from the mitochondria relies on the protease CLPP-1 (15) and the peptide exporter HAF-1 (16). Under healthy conditions, the transcription factor ATFS-1, which is unique for having both mitochondrial and nuclear targeting sequences, is transported into mitochondria and rapidly degraded. Under conditions of mitochondrial stress, perhaps because membrane potential and thus the efficiency of protein import into mitochondria are reduced, ATFS-1 is translocated to the nucleus (17,18). This change in ATFS-1 localization is a primary activator of the UPR^{mt}. Mitochondrial stress also causes the translocation of the transcription factors DVE-1 into the nucleus. In the nucleus, ATFS-1 works to increase transcription of aforementioned mitochondrial

quality control genes, as does DVE-1 in conjunction with UBL-5 (15,19,20). The activity of DVE-1 and UBL-5 are related to H3K9 dimethylation by MET-2 and its cofactor LIN-65 (20). Some results suggest that ATFS-1 and DVE-1/UBL-5/MET-2 are two separate branches of the UPR^{mt} (20), but how distinct they are, or whether some stressors activate one signaling branch but not the other, is unknown. Suppression of global transcription and selective upregulation of transcription of mitochondrial quality control genes also depends on histone demethylase JMJD-1.2 (20,21). The UPR^{mt} is best understood in *C. elegans*. Work in murine models, human cell culture lines, and patient samples from humans with mitochondrial genetic diseases are being used to investigate similar mechanisms in mammals (22,23).

Crucial mitochondrial quality control proteins including key chaperones HSP-60 and HSP-70, and proteases are conserved across species. ATFS-1 orthologs are upregulated upon mitochondrial challenges in mammals, as is FGF21, a secreted protein with roles in mitochondrial biogenesis and health, and is proposed component of the putative mammalian UPR^{mt} (24,25).

A growing body of work from our lab and others has shown hormesis from mitochondrial stress and the resulting activation of the UPR^{mt}. That is, while too great an amount of stress on mitochondria kills organisms prematurely, stress in a lower dosage range actually provides benefit to the organism by activating protective responses. Work in our lab has showed that in *C. elegans*, mitochondrial stress during the final stage of larval development turns on the UPR^{mt}, and increases the lifespan of the organism in a UPR^{mt}-dependent manner (26). This result has been replicated using a variety of mitochondrial stressors (20,21,27,28).

We have also shown that when neurons alone are subject to mitochondrial stress that activates the UPR^{mt}, they communicate this signal to distal tissues, activating the UPR^{mt} in a cell non-autonomous manner (20,21,26,27). Specifically, they signal to the intestine, which has liver-like metabolic functions in *C. elegans*. Mitochondrial stress to neurons and the resultant cell non-autonomous signaling replicates the hormetic effect of whole-animal stress, increasing the organism's lifespan (26). Additionally, work from our lab has shown that overexpression of the homolog of chromatin modifier PHF8 alone in neurons is sufficient to signal UPR^{mt} to distal tissues and recapitulate the hormetic effect as shown through lifespan extension (20,21).

C. elegans neurons have two main signaling routes: one is small clear vesicles (SCVs), which signal through classic neurotransmitters and biogenic amines, and the other is dense core vesicles (DCVs), which signal through neuropeptides (29). In a model using polyglutamate repeat overexpression to induce mitochondrial stress, cell non-autonomous signaling of the UPR^{mt} relied on the serotonin production gene tph-1 and dense core vesicle signaling. It is unknown whether other types of mitochondrial stress in neurons signal through these same components, or if stress-signaling components vary with type of stressor.

1.2 Mitochondrial DNA replication and related pathologies

When mitochondrial function is sufficiently compromised, an organism may develop a mitochondrial disease. Mitochondrial diseases in humans and mammal models often show striking tissue-specificity, even when they are the result of genetic mutations that exist in all cells in the organism. Post-mitotic tissues with high energy demands—that is, the nervous system and skeletal muscle—are often the most effected. These diseases frequently manifest as peripheral neuropathy and related hearing loss; epilepsy; severe, intractable depression; muscle-wasting; and sudden cardiac arrest. Liver failure and infertility are also frequently noted in the literature (24,30–38).

A common cause of mitochondrial genetic diseases is mutations in proteins affecting mitochondrial DNA (mtDNA) replication. Three proteins encoded in the nuclear genome act in concert to make the functional unit of the mtDNA replisome (Fig S1A): (i) DNA polymerase gamma (*POLG* in humans; *polg-1* in *C. elegans*), which elongates mtDNA; (ii) mitochondrial single-stranded binding protein (*mtSSB* in humans; *mtss-1* in *C. elegans*), a protein that binds the lagging strand and stimulates the activity of PolG; and (iii) Twinkle (*TWNK* in humans; *twnk-1* in *C. elegans*), the mtDNA replicative helicase. Twinkle is a recA/DnaB superfamily helicase, similar to the T7 phage replicative helicase, gp4 (39,40). In many metazoan species including *C. elegans*, Twinkle homologs lack the ancestral DNA binding and nucleotide hydrolysis domains necessary to the primase function. The ancestral N-terminal primase domain is connected by a linker region to the C-terminal helicase domain (40,41). *In vivo*, Twinkle monomers form a hexamer, making it a ring helicase, visible in electron micrographs (42–45). Human Twinkle unwinds DNA in a 5' to 3' direction, hydrolyzing dNTPs at the subunit interface, and leading the replisome complex (41). Mutations in PolG and Twinkle cause a variety of disease syndromes, which most often affect the nervous system and muscle, as previously noted (46).

Dominant mutations in PolG and in the Twinkle linker region lead to the accumulation of multiple mtDNA deletions in the muscle, heart, and brain, manifesting as progressive mitochondrial myopathy known as progressive external ophthalmoplegia (PEO) (31,33,34,36,44,47). This sometimes involves sensory neuropathy and parkinsonism (40,48). Molecular analyses reveal that in muscle and brain, PEO patients have an accumulation of large deletions in the mitochondrial genome. Breakpoints are often in regions that are thought to be difficult for polymerases, such as nucleotide runs and repeats (49). PEO, thus, exhibits the previously mentioned strikingly tissue-specific phenotypes.

Recessive mutations in PolG and Twinkle, as well as in proteins regulating dNTP pools, result in depletion of mtDNA, often in a tissue-specific manner. Recessive mutations in the Twinkle helicase region lead to infantile-onset spinocerebellar ataxia (IOSCA), which causes severe disability and is fatal within the first two decades of life (35,36,50). Our incomplete understanding of the mechanisms of these mitochondrial disease syndromes prevents the development of targeted therapies. In fact, there are no treatments for mitochondrial genetic diseases at this time. In order to further understand the molecular basis of these dysfunctions, animal models of genetically-induced mtDNA replication dysfunction are needed.

Over the last decade and a half, there has been an accumulation of evidence suggesting functional conservation of PolG and mtSSB in invertebrate models, including *D. melanogaster* (51–55) and *C. elegans* (56–59). There is also evidence supporting the role of Twinkle as a replicative helicase in *D. melanogaster* (60,61). While a Twinkle homolog with 36% identity to the human ortholog has been identified in the *C. elegans* genome (57,62), whether it functions as the mitochondrial DNA replicative helicase is unknown.

C. elegans possess a mitochondrial genome that is similar in size and structure to the mammalian mitochondrial genome, and shares most of the same genes (63). Additionally, major metabolic pathways and the major mitochondrial biogenesis pathway relying on PGC-1α are conserved, and similar age-related dysfunctions are observed in mammalian and nematode mitochondria. These include respiratory chain dysfunction, structural abnormalities, decreased oxygen consumption and ATP production, protein aggregation, and accumulation of mtDNA deletions, especially at repetitive sites (59,64–67). The conservation of replisome proteins and metabolic aging phenotypes, as well the genetic toolkit and ease of genetic and drug screening in this organism, makes *C. elegans* an appealing organism to model mtDNA diseases and to screen

for potential drug targets. Thus, I set out to investigate the role of the *C. elegans* Twinkle homolog. In chapter 3, I describe a project in which we used the model organism *C. elegans* to look at Twinkle homolog function in *C. elegans*, and the effects on mitochondrial health and stress when this protein is knocked out or knocked down. We hoped to eventually create a PEO disease model that we could use to interrogate tissue-specific differences in mitochondria induced by the mutation, screen for genes that protect mitochondrial health, and screen for drugs that suppress disease PEO disease phenotypes.

1.3 Mitochondrial stress and the *C. elegans* nervous system

The nervous system is comprised of two cell types: neurons and glia. Neurons are well known for their functions in receiving, synthesizing, and transmitting information. Glia were long overlooked by the neuroscience community who presumed they served only as metabolic support cells for neurons. Over the last decade and a half, new research has begun to illuminate the varied and essential roles of glial cells.

As the complexity of an organism increases, the ratio of glia to neurons increases. In the relatively simple animal *C. elegans*, the nervous system is comprised of 302 neurons and 56 glia (68). In, humans the ratio of neurons to glia is roughly one-to-one (69). In vertebrates, there many types of glial cells, of which astrocytes are the most numerous in the central nervous system (CNS) (69). Astrocytes are heavily processed cells, named for the star-like appearance their processes give them. A given astrocytes makes contact with multiple neurons and as many as tens of thousands of synapses (70). Their processes surround and contact neurons, especially at synapses. The functional unit of axon terminal, dendrite, and abutting astrocyte process is known as a tripartite synapse (71–73). Astrocytes are involved in synapse development, growth, and pruning, and modulate synaptic activity (71,74,75). They contribute to learning, cognition, and memory (75–80). They express neurotransmitter receptors, and release of neurotransmitters can regulate astrocyte function (81). Astrocyte inflammatory responses and dysfunction are features of, and may have causative roles in, CNS diseases such as Alzheimer's disease, amyotrophic lateral sclerosis (ALS), epilepsy, stroke, and traumatic brain injury (82–85).

While we are only at the beginning of understanding the roles of glia in C. elegans, some important insights have been gained in recent years, pioneered in large part by the Shiham lab (68,86–91). Similar to vertebrate neuronal development, *C. elegans* neurons and glia form from asymmetric cell divisions of neuroepithelial precursors. *C. elegans* glia are secretory and have essential roles in neuronal morphogenesis, structure, and function (87,90,92–94). *C. elegans* glia support neurogenesis, neuron process exploration and growth, and synaptogenesis, further supporting the hypothesis that the developmental relationship between glia and neurons is conserved between *C. elegans* and vertebrate models (68,87,91,92,95).

The nerve ring in *C. elegans* serves as the central neuropil and has the majority of the synapses in the animal. Four cephalic sheath (CEPsh) glial cells tile the nerve ring in a manner stereotypical to astrocytes. Similar in developmental process to vertebrate astrocytes, CEPsh glia start as simple bipolar cells and becoming highly branched, resembling the transition from radial glia to astrocytes (87,96,97). RNA sequencing experiments show that CEPsh glia are enriched for gene transcripts that are also enriched in mammalian astrocytes, including a homolog of the conserved astrocyte glutamate transporter GLT1 (*glt-1* in *C. elegans*) (89,91,98,99). CEPsh glia also express dopamine receptor and transporter homologs (89,100). The ensheathment of the nerve ring by CEPsh glia may serve as a sort of proto-blood-brain barrier, mediating contact between coelemic fluid and the neurons of the nerve ring (68,73,101). Fine processes of CEPsh

glia extend into the nerve ring, forming tripartite synapses (89). Amphid neurons run from the nerve ring to the most anterior part of the worm where they form the amphid sensillum, a sensory organ with roles in chemotaxis, mechanosensation, osmotaxis, and pheromone sensing (102). In addition to extensive contact with the nerve ring, CEPsh glia ensheath amphid neurons along their entire length, perhaps positioning glia to respond to the external world (103).

One of the technical challenges of uncovering glia function and distinguishing it from neuronal function is that they are so closely entwined, physically and functionally: glia in many regions of the brain in vertebrate model organisms provide crucial metabolic and trophic factors, without which neurons are not viable. While glia in *C. elegans* share many functions with mammalian glia, they are not necessary for neuronal survival (68,88,90,97). Thus, *C. elegans* provides unique opportunities to explore and dissect glia and neuron function.

As previously mentioned, our lab has shown that neurons play a special role in stress signaling in *C. elegans*: they are able to relay subcellular compartment-specific stress signals to distal tissues, activating stress response pathways—the UPR^{mt}, the endoplasmic reticulum unfolded protein response (UPR^{ER}), and heat shock response (HSR)—in a cell non-autonomous manner (20,26,27,50,104–106). Recently, our lab found that glia were able to activate the UPR^{ER} and transmit this signal to distal tissues (A. Frakes et al, manuscript forthcoming). In chapter 4, I describe the second major project of my thesis work. In this project, I examined the potential of glia to signal mitochondrial stress, the effects of this cell non-autonomous signaling on lifespan and stress resistance, and the signaling mechanisms of the pathway.

Chapter 2: Materials and Methods

Strains

The Bristol strain (N2) was used as wild type. The following worm strains used in this study were obtained from the *Caenorhabditis* Genetics Center (University of Minnesota) unless otherwise noted: VC2626 (*F46G11.1(ok3198)X*), VC1224 (*Y57A10A.15(ok1548)/mT1 II; +/mT1* [*dpy-10*(*e128)] II*), MQ887 (*isp-1*(*qm150*)*IV*), TK22 (*mev-1*(*kn1 III*)), CF512 (*rrf-3*(*b26*) *II*; *fem-1*(*hc17*) *IV*), SJ4005 (zcls4(hsp-4p::GFP)V), CL2070 (dvIn70[pCL25(*hsp-16.2p*::GFP, pRF4(*rol-6*))]), SJ4100 (*zcls13 V*[*hsp-6*::*GFP*]), and SJ410(*zcIs14[myo-3::GFP(mit)]*). We crossed SJ4005 (zcls4(hsp-4p::GFP)V), CL2070 (dvIn70[pCL25(*hsp-16.2p*::GFP, pRF4(*rol-6*))]), and SJ4100 (*zcls13 V*[*hsp-6*::*GFP*]) with the *hlh-17p::jmjd-1.2a* strain, whose generation is described below. We crossed VC2626 (*F46G11.1(ok3198)X*) with SJ4103 (*zcIs14[myo-3::GFP(mit)]*) to create the homozygozed line used in Chapter 3, Figure 6. Backcross of VC2626 (*F46G11.1(ok3198)X*) and cross with SJ4103(*zcIs14[myo-3::GFP(mit)]*) were confirmed with forward primer 5′-CCTTCTCCAAGACTTGACGC-3’ and reverse primer 5′-TACCCAGCGTATTGCACAAG-3’. We also used strains generated in the lab and previously published: AGD1505 (uthIs404[*myo-2p*::tdTomato, *sur-5p*::*jmjd-1.2a*::3'UTR *unc-54*]), AGD1510 (uthIs409[*myo-2p*::tdTomato, *rgef-1p*::*jmjd-1.2a*::3'UTR *unc-54*]). We also generated strains, as described below. Strains are available upon request.

Strain generation

For generation of *ptr-10p*::*jmjd-1.2a* animals, the 0.3kb upstream of the ptr-10 start codon was amplified from genomic DNA. For generation *fig-1p*::*jmjd-1.2a* animals, a 1264bp fragment upstream of fig-1 start codon was amplified from genomic DNA. For constructs with the hlh-17 promoter, a 3.0kb fragment upstream of the hlh-17 start codon was amplified from. For generation of *mir-228p*::*jmjd-1.2a animals*, a 2225bp fragment upstream of the *mir-228* start codon was amplified from genomic DNA (68,88). The *jmjd-1.2a* ORF was amplified from wild-type *C. elegans* cDNA. Full length DNA plasmid constructs were injected at 50 ng/µl along with a coinjection marker (*myo-2p*::tdTomato) at 2.5 ng/µl into SJ4100 (*zcls13 V*[*hsp-6*::*GFP*]) to generate transgenic overexpression nematodes. For integrated strains, animals with extra-chromosomal arrays were integrated by gamma irradiation and backcrossed 7x. Strains are available upon request.

Worm maintenance and RNAi

Worms were grown on solid agar nematode growth media (NGM) plates at 20°C on OP50 *E. coli* bacteria. For RNAi experiments, worms were fed HT115 *E. coli* bacteria carrying an RNAi construct or an empty construct, L4440, as empty vector control. Synchronized eggs were harvested by timed egg-lay (2 hours) or by bleaching worms with a solution of 1.8% sodium hypochlorite and 0.375 M KOH and grown on RNAi from hatch or L1 arrest. Bacterial feeding in RNAi experiments was conducted from hatch or L1 arrest, as indicated. RNAi strains were taken from the Vidal RNAi library if possible, and from the Ahringer RNAi library otherwise. All clones were sequence-verified.

Sequence analysis, alignment, and phylogeny

DNA and amino acid sequences were obtained from the National Center for Biotechnology Information (https://www.ncbi.nlm.nih.gov/) and Wormbase (https://wormbase.org/). DNA sequence analysis was performed using National Center for Biotechnology BLAST with standard settings. Amino acid sequence similarity was determined using National Center for Biotechnology BLAST with standard settings. Amino acid sequences were aligned using Clustal Omega software with standard settings, available from the European Bioinformatics Institute (https://www.ebi.ac.uk/Tools/msa/clustalo/). We visualized this alignment using the TCoffee Expresso tool, available at tcoffee.crg.cat. For the phylogenetic tree, sequences were analyzed using Phylodendron, set to create a phenogram with horizontal tree growth with node lengths and inner nodes. This software is available from Indiana University's Bio-Archive (http://iubio.bio.indiana.edu/treeapp/treeprint-form.html).

in silico modeling of Twinkle

Sequences of Twinkle homologs for alignment and modeling were retrieved from UniProt database. Multiple sequence alignment was done using Promals3D server (http://prodata.swmed.edu/promals3d/). 3D homology models for C-terminal helicase domain of human and *C. elegans* TWINKLE proteins were done in Swiss-Model server using alignment mode. Structural analysis, protein superimposition and figure preparation were done using Discovery Studio v3.5 (BioVia) software.

Brood size assay

Brood size assay performed as described (107) with some modifications. Briefly, animals were grown on RNAi from hatch. 10 L4 animals per condition were moved to individual plates, and then moved again every 12 hours. When animals were removed from plates, plates were put at 4° C so eggs would not hatch, and then eggs were counted. Experiment was done in two biological repeats. Statistical significance was calculated using a one-tailed t-test.

Motility assay

Motility assay was performed as described (108) with some modifications. Briefly, worms were synchronized by timed egg lay, and grown on RNAi bacteria from hatch. Worms were picked at random from a plate into 50 uL of M9 on an empty plate, and 25 seconds of video was captured immediately. Body bends were counted by eye for each worm; $N \geq 9$ worms/strain/experiment were counted. Experiment was done in three biological repeats. Statistical significance was calculated using a two-tailed t-test.

Oxygen consumption rate

Oxygen consumption rate of whole worms was measured as described (109) with some modifications. Briefly, worms were washed from plates and incubated in M9 for 20 minutes to remove residual bacteria. Then, $N \geq 50$ worms (10 worms/ well) were transferred to the Seahorse XF96 Cell Culture Microplate (Agilent Technologies, 101085-004) in a total volume of 180 uL. Oxygen consumption rate per well was measured five times using the Seahorse XFe96 Analyzer

(Agilent Technologies). Experiment was done in three biological repeats. Statistical significance was calculated using a two-tailed t-test.

Adult UV stress resistance assay

Resistance of adult nematodes to UVC was performed as described (110), with some modifications. After completing egg-laying (D6), animals were treated with 1200 J/m^2 at D6, and then moved to fresh plates. Irradiation was performed using a CL-1000 Ultraviolent Crosslinker (UVP, CL1000). N≥50 animals per genotype. Survival was scored every 24 hours after. This assay was performed once.

Larval UV stress resistance assay

Larval UV stress resistance assay was performed as described (111), with some modifications. Briefly, animals were bleached, and eggs were left in M9 for 24 hours to achieve L1 arrest. Animals were put on NGM plates without OP50 bacteria, and treated with 10 J/m^2 at 24, 48, and 72 hours, and then moved to plates with standard OP50 food. Irradiation was performed using a CL-1000 Ultraviolent Crosslinker (UVP, CL1000). Development to L4 or adulthood was scored every 24 hours. N≥33 per condition. Statistical significance was calculated using a one-tailed t-test.

Heat shock response (HSR) assay

HSR was induced by putting D1 animals at 34°C for two hours, recovering at 20°C for four hours, and then imaging as described below. RNAi against critical HSR chaperone *hsf-1* was used as a negative control.

Endoplasmic reticulum unfolded protein response (UPR^{ER}) assay

UPR^{ER} was induced putting animals on RNAi targeting *tag-335*, which we found induced this response in a screen for inducers of the UPR^{ER}. Animals were grown on RNAi from hatch, and imaged at D1. RNAi against critical UPR^{ER} component *xbp-1* was used as a negative control.

Microscopy of whole animals

Synchronized animals were obtained through timed egg lays. For all imaging, unless otherwise noted, animals were D1 adult hermaphrodites and experiments were performed in triplicate with at least 8 animals imaged per experiment. Worms were synchronized by timed egg lay or bleaching, and grown from hatch on RNAi bacteria when RNAi was used. For fluorescent microscopy, animals from a population were chosen at random under the light microscope. All images were taken using a fixed exposure and gain to just below saturation for the intestinal fluorescence. Images were taken in at least two biological repeats. Animals were anaesthetized with 0.1 M sodium azide (Fisher Scientific, 26628-22-8), and imaged immediately with a Leica MDG41 Stereoscope and Leica DFC3000 G Camera.

Microscopy of muscle mitochondria

Imaging was performed as described (7), with some modifications. Briefly, synchronized animals were obtained through timed egg lay. For all imaging, animals were D1 adult hermaphrodites and experiments were performed in triplicate with 10–20 animals imaged per experiment. Worms were grown from hatch on RNAi bacteria. Animals were placed directly in M9 media on a glass slide without anesthesia, and imaged immediately (modification courtesy of G. Garcia). Single-plane images of muscle mitochondria from cells just anterior to the vulva were captured in each worm using a Zeiss Oberserver.Z1 Axiovert microscope equipped with a Zeiss axiocam 506 camera, lumencor sola light engine, and ZenBlue software. GFP was visualized by using a 63x/1.4 Plan Aprochromat objective and a standard GFP filter (Zeiss filter set 46 HE). Experiment was performed in more than three biological repeats.

Microscopy of *dve-1p*::*dve-1*::GFP localization

Briefly, synchronized animals were obtained by bleaching adults. For all imaging, animals were D1 adult hermaphrodites and experiments were performed in triplicate with 10–15 animals imaged per condition per experiment. Worms were grown from hatch on RNAi bacteria.
Worm Fixing Protocol and Sample Imaging for confocal microscopy: worms were grown on the RNAi specified from hatch, and at D1, they were rinsed off plates with M9 and added to 15-mL conical tubes. Animals were washed 3x with M9 to remove bacteria, then transferred to microcentrifuge tubes using a glass Pasteur pipette. M9 was aspirated to 100 µL, and 400 µL of PBS-buffered paraformaldehyde was added directly to worms. Tubes were rocked at room temperature for 10 minutes. Worms were pelleted by centrifuging for 2 minutes at 1000g, and liquid was aspirated leaving ~100 µL. Animals were then frozen at 80°C.
After thawing, animals were washed 3x with PBS. Next, 1 mL PBS and 0.5 uL DAPI were added to the sample, which was rocked at room temperature for 1.5 hours, and then washed 3x in PBS. As much liquid as possible was aspirated, and 100 uL of 75% glycerol buffered in PBS was added. Animals were stored at 4°C until being imaged. For imaging, samples were mounted directly on glass slides, a coverslip was placed directly on the specimen, and sealed with nail polish. Mounted slides were kept at 4°C for at least 12 hours prior to imaging to allow for settling of specimen and rehydration with glycerol. Imaging was performed as described (7), with some modifications. Z-stack images of intestinal nuclei from the hindgut in each worm were captured using a Zeiss Oberserver.Z1 Axiovert microscope equipped with a Zeiss axiocam 506 camera, lumencor sola light engine, and ZenBlue software. GFP was visualized by using a 40x/1.4 Plan Aprochromat objective and a standard GFP filter (Zeiss filter set 46 HE) with an exposure of 110 ms. Experiment was performed in three or more biological repeats. I thank Gilbert Garcia and Dr. Joseph Daniele for this protocol.

Electron microscopy

Samples were prepared as described (112), with some modifications. Briefly, 200-300 worms were grown on RNAi bacteria from L1 arrest, and then loaded into specimen carriers and fixed using high pressure freezing (Balzers HPM 010 High Pressure Freezer). Samples were then freeze substituted in 1.0% osmium tetroxide, and 0.1% uranyl acetate in acetone at −90°C, and then warmed to −10°C and washed with pure acetone. Worms were embedded in increasing concentrations of Epon resin at room temperature, transferred to flat bottom embedding capsules in pure resin, and cured at 65°C for 48h. Serial sections were cut at 70cnm, and placed onto

formvar coated mesh copper grids, and imaged using a FEI Tecnai 12 Transmission electron microscope. Experiment was performed once.

Quantitation of fluorescence by whole animal sorting

Quantitation of fluorescence along the length of the worm was performed as described (113)**.** Briefly, we used a Union Biometrica complex object parameter analysis sorter (COPAS) Biosorter (product no. 350–5000–000) using 561 nm and 488 nm light sources. The Biosorter was flushed with 10% bleach, M9 buffer, COPAS cleaning solution (#300–5072–000), and then worms in M9 buffer were added to the cup. Data was acquired using optimized settings for laser PMT power and size gating. Worm profile data was collected using the Biosort 5401.1 software provided with the Biosorter machine. Data analysis, significance testing, and data plotting was run using the LAMPro Suite graphical interface to run MATLAB scripts (version R2015a).

RNA purification and qRT-PCR

RNA purification were performed as described (21), with minor modifications. Briefly, mixed age populations of C. elegans were age synchronized by egg bleaching and cultivated on NGM plates. Animals were collected in M9 buffer, centrifuged at 1,000x g for 30 seconds, resuspended in Trizol (Life Technologies, 10296-028), and snap frozen in liquid nitrogen. After several freeze-thaw cycles, total RNA was isolated using chloroform and isopropanol. 1 µg of total RNA was subjected to cDNA synthesis using the QuantiTect Reverse Transcription Kit (Qiagen, 205314). Quantitative real-time PCR reactions were performed with the SYBR Select Master Mix (Life Technologies, 4472920) in Optical 384-well MicroAmp plates (Life Technologies, 4309849) using a QuantStudio 6 Flex (ThermoFisher). *pmp-3* (forward primer 5'-CGGTGTTAAAACTCACTGGAGA-3', reverse primer 5'-TCGTGAAGTTCCATAACACGA-3'), *cdc-42* (forward primer 5'-AGGAACGTCTTCCTTGTCTCC-3', reverse primer 5'-GGACATAGAAAGAAAAACACAGTCAC-3'), and Y45F10D.4 (forward primer 5'-AAG CGT CGG AAC AGG AAT C-3', reverse primer 5'-TTT TTC CGT TAT CGT CGA CTC-3') were used as housekeeping genes; forward primer 5'-GAT CCT CCA TTG GAT GCT TG-3' reverse primer 5'-CGG AAG TTT GAT GCC ATT TT-3' were used to detect *twnk-1*. Experiment was performed once.

Quantitation and analysis of mitochondrial DNA content

Worms (N=10) were lysed in 15 uL of buffer as previously described (58). The product was diluted 1/1000, and 1 uL of the resulting product was used for each reaction. Absolute quantitation was performed as described (56). Briefly, each experiment included a series of dilutions of pCR2.1 plasmid with the mtDNA NADH dehydrogenase subunit 1 (*nd-1*) sequence inserted. This plasmid was a gift from Dr. A. Trifunovic. Primers for NADH *nd-1* were used to detect the plasmid *nd-1* sequence as well as mtDNA in samples (*nd-1* forward primer is 5′-AGCGTCATTTATTGGGAAGAAGAC-3′ and reverse primer 5′-AAGCTTGTGCTAATCCCATAAATGT-3′). Samples were loaded in triplicate, and absolute quantity of mtDNA was calculated in reference to the Ct values of the plasmid reference. Absolute quantities are displayed as relative to N2 on OP50 or EV RNAi, respectively, at D1. Experiments were done in at least two biological repeats of each experiment. Statistical significance was calculated using a one-tailed t-test.

Lifespan assay

Lifespan experiments were conducted at 20°C as previously described (26). Briefly, lifespans were performed on nematodes fed HT115 bacteria expressing the indicated RNAi, using the pre-fertile period of adulthood as day 0. Animals were transferred to fresh plates every other day until day 12.), GraphPad Prism 6 for Mac OS X (GraphPad Software, Inc.), was used for statistical analysis to determine significance calculated using the log-rank (Mantel-Cox) method. For lifespans done with paraquat, paraquat was added to the media to the specified quantitation before the plates were poured.

Paraquat stress resistance

Acute paraquat stress resistance assays were conducted as previously described, with some modifications (114). Briefly, animals were grown from hatch on empty vector L4440 bacteria or bacteria expressing RNAi against *daf-2* which served as a positive control. At D1, worms were submerged in 50ul of 0.4M paraquat dissolved in S-basal buffer at 20°C. Death was determined on every two hours by the lack of movement after prodding with a platinum wire. Experiment was carried out for 10 hours. 60 worms were used for each condition in each experiment.

Statistical analysis and figure generation

T-tests to analyze significance of data were performed using Sheets (Google). Figures were made using R (RStudio, 1.1.453), GraphPad Prism 6 for Mac OS X (GraphPad Software, Inc.), and Adobe Illustrator CC 22.1 (Adobe).

Chapter 3: Twinkle is not required for mtDNA replication in *C. elegans*, but may have alternate mitochondrial functions

3.1 Introduction

In mammals, PolG, Twinkle, and single-stranded binding protein (mtSSBP) form a conserved minimal mtDNA replisome (38). In addition to these components, mtDNA maintenance requires the presence of topoisomerases, endonucleases and the transcription factor TFAM, as well as mitochondrial histones that package the supercoiled mtDNA into mitochondrial chromosomes (115).

Twinkle and TFAM are the known mtDNA copy number regulators in mammals, the former regulating entry of mtDNA into replication, and the latter binding mtDNA in a histone-like manner, and increasing mtDNA half-life (32,116). Knockout of Twinkle and other mtDNA maintenance proteins shows that these proteins are essential for embryonic development in mice (117). *D. melanogaster* has a conserved Twinkle homolog, which is also an independent regulator of mtDNA copy number (118). Twinkle levels affect replication speed and fidelity in both flies and mice (116,119). These findings strongly suggest that Twinkle is a conserved mtDNA replicative helicase, licensing mtDNA to enter replication in both vertebrate and invertebrate metazoans. In the yeast *S. cerevisiae*, however, there is no Twinkle homologue, indicating its later evolutionary emergence, or loss in this organism (120).

In this work, we investigated the function of the *C. elegans* Twinkle homolog by examining not only mtDNA content, but conducting a variety of assays of mitochondrial function and stress in order to better understand the function of this protein in *C. elegans*.

3.2 Results

Twinkle evolved from the T7 phage gp4 helicase protein, and is found in most eukaryotes, with fungi being a notable exception (41). DNA sequence analysis of the *C. elegans* genome confirmed one Twinkle homolog, *F46G11.1*, which we named *twnk-1*. Phylogenetic analysis of Twinkle proteins in other model organisms showed that the nematode branch has significantly diverged from the mammalian branch, as well as from that of other model organisms (Fig 1A). The degree of identity between the human and mouse homologs of Twinkle at the polypeptide level is about 85%; identity between human Twinkle and invertebrate model homologs is about 35-40% (40). In *C. elegans* and *C. briggsae*, *twnk-1* carries a 27 amino acids (AA) insertion (Fig 1B).

Next, we focused on the functional C-terminal helicase domain. We observed similarities in the amino acid sequence across species in key regions. Overall, the degree of amino acid sequence similarity to the human homolog in *twnk-1* (36% identity) is comparable to that of the worm homolog of PolG, *polg-1* (37% identity*),* which is functionally conserved (56,58,59). Our

sequence analyses identified no other putative Twinkle homologs or pseudogenes in *C. elegans*. To further examine whether sequence differences would affect the function of the protein, we used *in silico* modeling of the helicase domain to predict its structure. This analysis indicated that the 27 AA insertion is in the first DNA binding loop, likely at the surface where subunits interact (Fig 1C). Despite possible disruptions to the DNA binding, we continued our characterization, as this insertion may have an adaptive role, such as altering the preference to specific DNA binding motifs.

To further confirm *twnk-1* as the functional homolog of Twinkle, we attempted to detect the TWNK-1 protein in mitochondria by quantitative liquid chromatography-mass spectrometry of isolated *C. elegans* mitochondria. We were unable to detect POLG-1 or TWNK-1, suggesting that they exist at levels beneath the detection limits of this method (data not shown). Because of the detection limits, we did not pursue this route of inquiry further. By expressing a TWNK-1 tagged with an mRuby fluorophore under a highly expressed all-tissues promoter (*sur-5p*), we confirmed that the protein localizes to the mitochondria in *C. elegans*, despite lacking a canonical mitochondrial targeting sequence (Fig 1D).

Loss of *twnk-1* does not deplete mitochondrial DNA

To functionally investigate the role of *twnk-1* in worms, we used RNAi knockdown of *twnk-1*, as well as a knockout strain from the Vancouver consortium (VC2626 (*F46G11.1(ok3198) X*)). In this strain, portions of the N-terminal primase region, the entire linker region, and the Walker A nucleotide binding motif of the C-terminal helicase domain have been deleted (Fig S1B). The resulting truncated mRNA is likely degraded by nonsense-mediated decay (121). Indeed, we were able to confirm the presence of *twnk-1* transcripts in larval wild type worms, but not *twnk-1* mutant animals (data not shown). We conclude that *twnk-1* is an actively transcribed component of the genome in wild type animals, and that in *twnk-1* mutant animals, no or undetectable levels of *twnk-1* mRNA are allowed to persist.

We predicted that if Twinkle is functionally conserved in *C. elegans*, this strain should suffer from inhibited mtDNA replication. Research in human cell lines confirms that loss of Twinkle is sufficient to deplete mtDNA (32), while Twinkle overexpression in mice is sufficient to increase mtDNA copy number (32,116). We examined the effect of loss of *twnk-1* on mtDNA levels in *C. elegans*. Previous work showed that mtDNA content approximately doubles by day 5 of adulthood (D5) in N2 (wild-type) worms. In contrast, when *polg-1* and the mtSSBP homolog *mtss-1* were knocked down by RNAi, mtDNA levels on D5 decreased to less than half of their day 1 of adulthood (D1) levels, suggesting functional conservation of these genes with their human homologs (57). We replicated these findings, and showing that knockdown of *polg-1* and *mtss-1* significantly decreased the levels of mtDNA by D5, despite similar mtDNA levels on D1. We also tested the effects of knocking down the TFAM homolog, *hmg-5*, a key activator of mitochondrial transcription that is also crucial for mtDNA replication and mtDNA copy number. Knockdown of *hmg-5* had a similar effect to *polg-1* and *mtss-1*, causing a comparable decrease in mtDNA by D5 (Fig 2A). However, neither RNAi knockdown or knockout of *twnk-1* caused loss of mtDNA in mid-adulthood (Fig 2A, 2B). Furthermore, mtDNA levels of *twnk-1* mutants and animals treated with *twnk-1* RNAi were both higher than the control at D1, and further increased at D5 (Fig 2A, 2B). While these results demonstrate that loss of *twnk-1* does not cause the expected loss of mtDNA as replisome components, *polg-1* and *mtss-1*, the increase in mtDNA upon loss of *twnk-1* may indicate a connection to other mitochondrial functions.

To further elucidate the role of *twnk*-1 in mitochondrial DNA replication, we tested the recovery of worms following radiation stress. UV stress in *C. elegans* has been shown to induce mitophagy and loss of mtDNA, and recovery from UV stress requires mtDNA replication (111). While we found that adult *twnk-1* animals survived UV stress as well as adult wild type animals (Fig S2), *twnk-1* larval animals were compromised in their ability to recover from UV stress relative to wild type animals, though this effect did not reach statistical significance (Fig 2C). Thus, our results indicate that *twnk-1* function does not dampen normal mtDNA replication or affect UV stress survival in adulthood, but may impair recovery from a stress that requires mtDNA replication during larval development.

Loss of *twnk-1* does not impair mitochondrial function, but causes stress phenotypes

We next focused on mitochondrial function at the organelle level. If *twnk-1* is functionally conserved, loss of *twnk-1* would be expected to reduce mitochondrial health and metabolic function. To this end, we analyzed oxygen consumption rate (OCR) in early and mid-adulthood. While at individual time points, loss of *polg-1* nor *twnk-1* resulted in significant changes in OCR, the direction of these changes relative to N2 was variable. Taken together, these data suggest that there is no net change in OCR upon loss of *twnk-1* or *polg-1* (Fig 3A and S3A). Conversely, knock down of mitochondrial ribosome protein subunit 5 (*mrps-5*) consistently showed a significant reduction in OCR.

Dysfunction at the organelle level may activate the mitochondrial unfolded protein response (UPR^{mt}), a protective transcriptional regulation program activated upon mitochondrial stress. In a murine model of Twinkle mutation, critical and conserved UPR^{mt} proteins, including the canonical mitochondrial chaperone protein mtHSP-70 (HSP-6 in *C. elegans*), are upregulated (122). Thus, we assayed whether loss of *twnk-1* and other replication-related proteins activated this response by imaging the expression of an *hsp-6*::GFP transcriptional reporter for UPR^{mt} activation. We observed a mild activation of the reporter upon knockdown of *twnk-1*; knockdown of *polg-1*, *mtss-1*, and the TFAM homolog *hmg-5* caused a more subtle induction of this response (Fig 3B, 3C). In case the maternal contribution of these proteins was buffering the animals from dysfunction and stress, we followed animals through two generations of RNAi treatment, but did not see increased reporter activation in the second generation (Fig S3B). Thus, while neither loss of *twnk-1* or disruption to replisome function is a potent activator of the UPR^{mt} in *C. elegans* as assayed by *hsp-6*::GFP, some stress response was evident upon knockdown of *twnk-1*, similar to the level we see caused by expression of expanded repeating glutamates in a *C. elegans* model of Huntington Disease type protein aggregation (27).

To determine whether *twnk-1* affects metabolic functions of mitochondria, we tested whether loss of *twnk-1* would cause synthetic phenotypes with other perturbations to mitochondrial function. Using RNAi to knockdown electron transport chain (ETC) components, *isp-1* (Complex III) and *cco-1* (Complex IV), we saw no obvious synthetic effects on development, reproduction, or movement in *twnk-1* animals relative to wild-type animals (Fig 3D). In a reciprocal experiment, knockdown of *twnk-1* in ETC complex III mutant, *isp-1*, and ETC complex II mutant, *mev-1*, did not have obvious synthetic effects (Fig 3E). Beyond ETC functions, we hypothesized that oxidative metabolism may be impaired, which would make *twnk-1* mutant animals rely more heavily on glycolysis. To investigate whether *twnk-1* mutants show this metabolic pattern, we knocked down four genes crucial for glycolysis. *twnk-1* mutants showed no gross synthetic effects on development, reproduction, or movement when subject to

RNAi knockdown of glucose transmembrane transport gene *fgt-1*, hexokinase genes *hxk-1* and *hxk-2*, or putative triosephosphate isomerase *tpi-1* (Fig 3F, 3G).

Next, we examined mitochondrial morphology, as it may reflect organelle health. Mitochondria in muscles are the most accessible for imaging in worms: in wild-type animals, they exist in lace-like networks through the myocyte. We previously found that overexpressing GFP in mitochondria sensitizes them to fragmentation (unpublished data). Using a strain expressing GFP targeted to mitochondria in muscles, we observed that while mitochondrial networks remained intact in the control, when *polg-1* is knocked down or *twnk-1* is mutated, the mitochondrial network in a subset of muscle cells is fragmented in a stereotypical stress pattern (Fig 4A). The mosaicism of this phenotype is consistent with how muscle dysfunction manifests in human mitochondrial myopathies, where some muscle cells appear normal, and others show loss of ETC function, and disruptions to mitochondrial morphology (25,33,122–124). To examine the morphology of individual mitochondria in greater detail, we used high magnification transmission electron microscopy on animals at D1 of adulthood (Fig 4B). In diseased patients, mouse models, and *polg-1* mutants, swollen mitochondria with concentric cristae have been observed (33,50,56,125). We observed no disruptions to mitochondrial cristae upon loss of *polg-1* or *twnk-1*.

Loss of *twnk-1* does not affect development or decrease muscle function, but decreases reproductive capacity

We continued our characterization of loss of *twnk-1* function on organismal health by examining whether *twnk-1* animals exhibited a developmental delay, as mitochondrial biogenesis is crucial for larval development. We found that *twnk-1* animals reached the last larval stage (L4) and the first day of adulthood (D1) concurrent to age-matched wild type worms (Fig 5A). In addition, loss of *twnk-1* showed no synthetic developmental effects with impaired mtDNA replisome function caused by RNAi knockdown of *polg-1* (Fig 5B). The reproductive capacity of the worms was of interest, as *C. elegans* egg production requires robust mitochondrial biogenesis (58). *twnk-1* animals had a reduced brood size relative to N2 animals on empty vector or *polg-1* RNAi (Fig 5C), an effect we also observed informally during strain maintenance. Next, we examined whether loss of *twnk-1* affected muscle function, as loss of mitochondrial function has been linked to decreased muscle function, which worsens with age (56). We found that rate of movement in liquid (thrashing) in early and mid-adulthood was not reduced in *twnk-1* animals (Fig 5D; replicates shown in Fig S5); in fact, these animals maintained their rate of thrashing better than wild type animals in mid-adulthood. This may be related to our finding that *twnk-1* animals have higher mtDNA levels. In summary, loss of *twnk-1* does not seem to negatively impact development and in fact preserves muscle function, but does decrease fecundity.

Screening for the functional homolog of Twinkle

Finally, as our results suggested that *twnk-1* is not functioning as the primary mtDNA replicative helicase in *C. elegans*, we sought to determine if another helicase has this function. We screened a library of RNAi clones, which represents >90% of the known RNA and DNA helicases in *C. elegans* (124 in total). In our primary screen, we looked for synthetic effects on development or fertility in combination with mutations in *twnk-1*, *polg-1*, and ETC component, *isp-1*, with wild type animals and a common sperm-deficient sterile strain as a control. The results of these screens are summarized in Figure 6 (see also Supplementary Table 1). Finally,

we screened initial hits and individually selected candidate genes for reduced mtDNA level; this yielded no promising leads for an alternate mtDNA replicative helicase.

3.3 Discussion

In this work, we set out to determine whether *twnk-1* is the functional homolog of Twinkle, as an extension of previous works that established conservation of the other integral components of the mtDNA replisome. We found, however, that the worm Twinkle homologue *twnk-1* does not appear to function as a replicative helicase for mtDNA, making *C. elegans* an exception in multicellular eukaryotes.

Analyzing the TWNK-1 amino acid sequence in *C. elegans* revealed a similar degree of conservation to the human homologue as was observed between the human and worm PolG, which is functionally conserved. We were further encouraged by the *in silico* modeling of the structure of TWNK-1, which indicated similarity in the C-terminal helicase domain, and the localization of TWNK-1::mRuby to the mitochondria. However, animals with knockdown or knockout of *twnk-1* were viable and did not show loss of mtDNA or decreased oxygen consumption, contrary to the detrimental phenotypes of knock-down of other replisome components. These results indicate that *twnk-1* lacks functional conservation with the human homolog.

In fact, upon loss of *twnk-1*, mtDNA was slightly, but significantly, elevated, suggesting that *twnk-1* may functions in non-replicative mtDNA processing, such as repair, or that increased mtDNA is the result of a secondary response, such as mitochondrial biogenesis spurred by stress. Following UV stress in *C. elegans*, mitochondria and mtDNA are degraded by mitophagy. In order to recover from this acute stress, cells undergo a burst of mitochondrial biogenesis and mtDNA replication (111). *twnk-1* mutant adults were not sensitive to UV stress, but worms in the first larval stage (L1) had reduced resistance to UV stress. These results suggest that *twnk-1* may have acquired a role as a repair- or stress-specific helicase during development. *twnk-1* mutants also show reduced fecundity. As oocyte production requires a surge in mitochondrial biogenesis (58), this result may be associated with a deficiency in some kind of mitochondrial function.

The hypothesized genetic interaction of *twnk-1* with different cellular pathways, including other replisome components (*polg-1*), glycolysis (*hxk-1*, *hxk-2*, *fgt-1*, *tpi-1*), and oxidative phosphorylation (*isp-1*, *mev-1*, *cco-1*), revealed no synthetic developmental or physiological defects, which is consistent with *twnk-1* not having a role in respiratory chain function or nutrient metabolism. Interestingly, knocking down *spg-7*, the *C. elegans* homolog of the mitochondrial quality control protease paraplegin, caused developmental arrest of the *twnk-1* mutant. *spg-7* is the *C. elegans* homolog of the mitochondrial quality control protease, parapalegin; its synthetic interaction with *twnk-1* may suggest a prior challenge to the mitochondrial protein landscape, or indicate that *twnk-1* is related to managing mitochondrial stress. Finally, imaging of muscle mitochondria revealed that knockdown of *twnk-1* causes the mitochondrial network to fragment, a classic indicator of mitochondrial stress in *C. elegans* (7). Taken together, our results indicate that TWNK-1 has a pleiotropic role in regulating mitochondrial form and function distinct from mtDNA replication in *C. elegans*.

An indication for possible such role may be a finding in human cell lines, where Twinkle maintains its punctate mitochondrial localization and association with the inner mitochondrial membrane (IMM) even in cells lacking mitochondrial DNA (P_0); this is in marked contrast to other replisome proteins, which are diffuse in the absence of mtDNA (40,126,127). Specifically, human Twinkle was found to associate with cholesterol in the IMM (Gerhold *et al.*, 2015) .

Additionally, mammalian cell culture models show that constriction of the IMM is an important early step in mitochondrial fission (128), and preferentially occurs where the replicating mtDNA nucleoid is located (129). The morphological and physiological defects we observed upon loss of *twnk-1* may imply that, in *C. elegans*, Twinkle serves as an IMM protein that is important to mitochondrial membrane structure, and organelle morphology and dynamics. While research on Twinkleopathies has focused on loss of replicative functions, our findings suggest that it may be worth investigating whether other kinds of mitochondrial distress are also causative in these syndromes. We hoped to examine the effect of expressing human Twinkle in *C. elegans*, but were unable to confirm successful overexpression of human Twinkle in *C. elegans*, or generate viable animals expressing a dominant mutation in the linker region (PEO type) of human Twinkle (data not shown).

We conclude that *C. elegans* is an evolutionary divergence from the typical metazoan mtDNA replisome, likely having recruited the conserved Twinkle protein to alternative mitochondrial tasks. Finally, we screened dozens of other helicases but were unable to find one that appeared to be functioning as an alternative primary mtDNA replicative helicase. Investigations of additional genes may find a functional homolog of Twinkle in *C. elegans*, and set the stage for modeling mtDNA diseases in this organism.

3.4 Figures

Figure 1: Phylogeny, sequence alignment, and structural analysis of Twinkle homologs

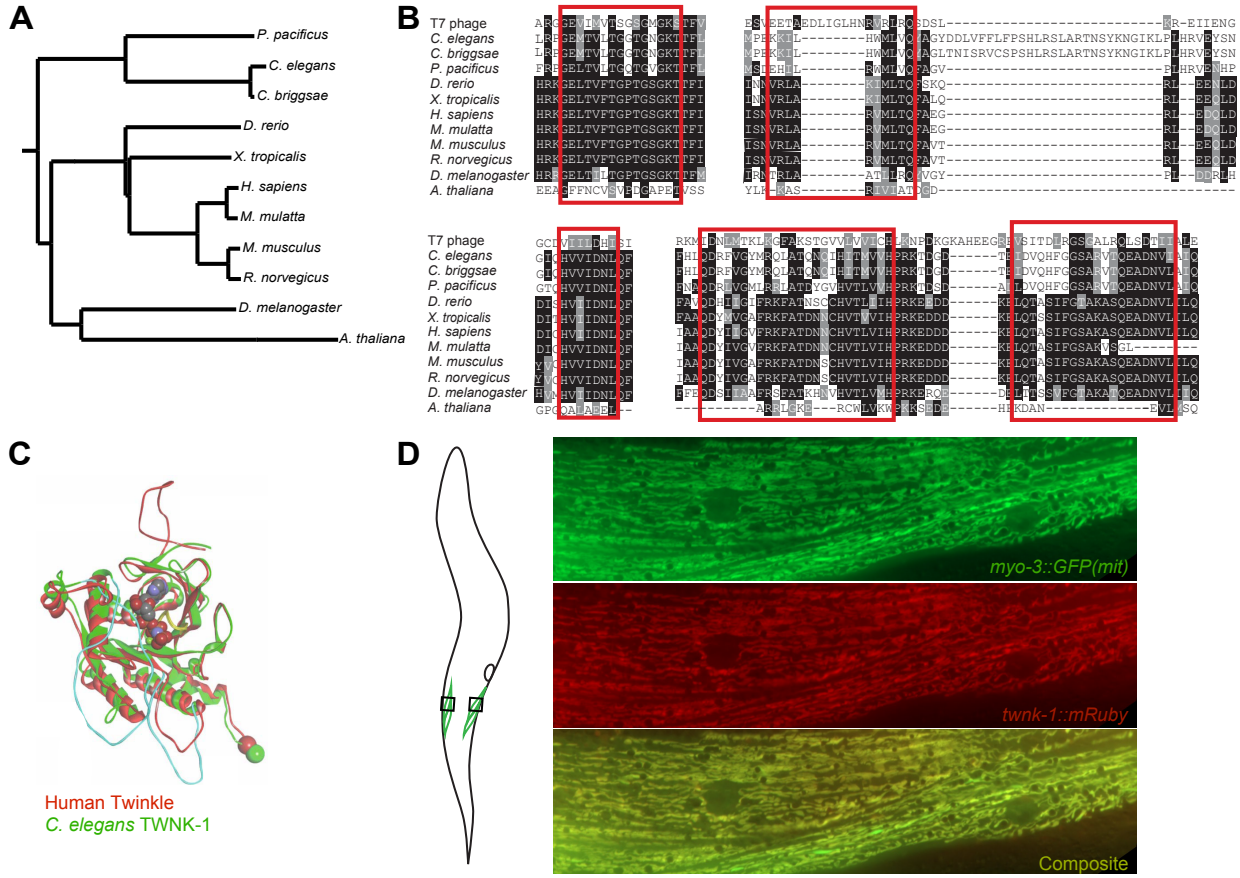

Figure 1: Phylogeny, sequence alignment, and structural analysis of Twinkle homologs (A) *Phylogenetic tree of twinkle homology:* Phylogenetic tree of model organisms was constructed according to AA sequence of Twinkle homologs or predicted Twinkle homologs. (B) *Sequence alignment of the C-terminal helicase region:* The sequence of the C-terminal helicase region from different species was aligned. Identical (black) and similar (gray) residues in key regions (red boxes) are highlighted. (C) in silico modeling of Twinkle: Structure model and overlay of the C-terminal helicase region of human (red) and C. elegans (green) Twinkle, with ATP in the Walker A binding cleft. (D) Illustration shows where on the worm body micrographs were taken. Micrographs show localization of TWNK-1::mRuby in myocytes; GFP genetically targeted to muscle mitochondria is used as a mitochondrial marker.

Figure 2: Loss of *twnk-1* increases mtDNA, but decreases fitness under mtDNA replicative stress.

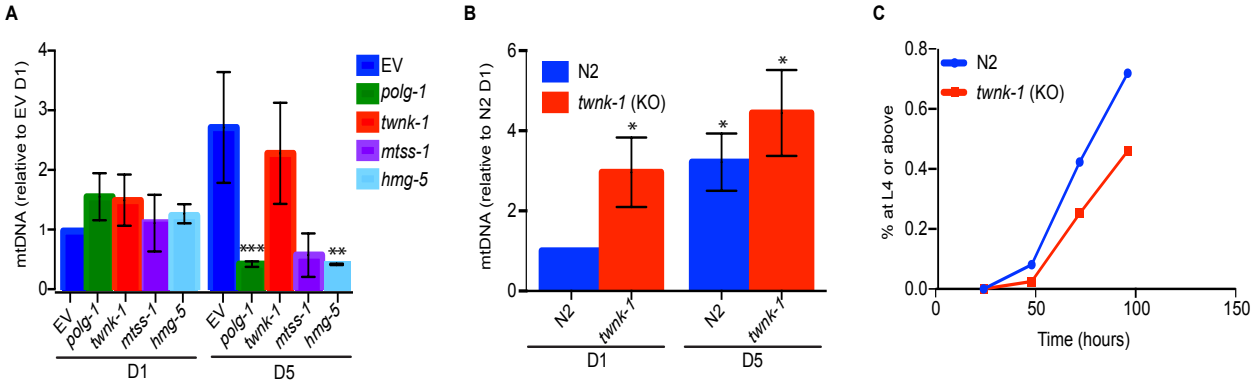

Figure 2: Loss of *twnk-1* increases mtDNA, but decreases fitness under mtDNA replicative stress. (A*) mtDNA levels in twnk-1 knockdown*: Ratio of absolute quantity of mtDNA of animals on replisome component and *hmg-5* RNAi, relative to empty vector at D1, as measured by qPCR. Results shown as mean ± SEM, *** $p < 0.001$, **$p < 0.01$, *$p < 0.05$; ns, $p > 0.05$. (B) *mtDNA levels in twnk-1 mutants:* Ratio of absolute quantity of mtDNA in wild type versus *twnk-1* animals, relative to wild type animals at D1, as measured by qPCR. Results shown as mean ± SEM, ***$p < 0.001$,**$p < 0.01$,*$p < 0.05$; ns, $p > 0.05$. C) Mutation in *twnk-1* decreases resistance to UV radiation: Effect of UV treatment on larval development in wild type and *twnk-1* animals.

Figure 3: Loss of *twnk-1* causes no gross defects in mitochondrial function.

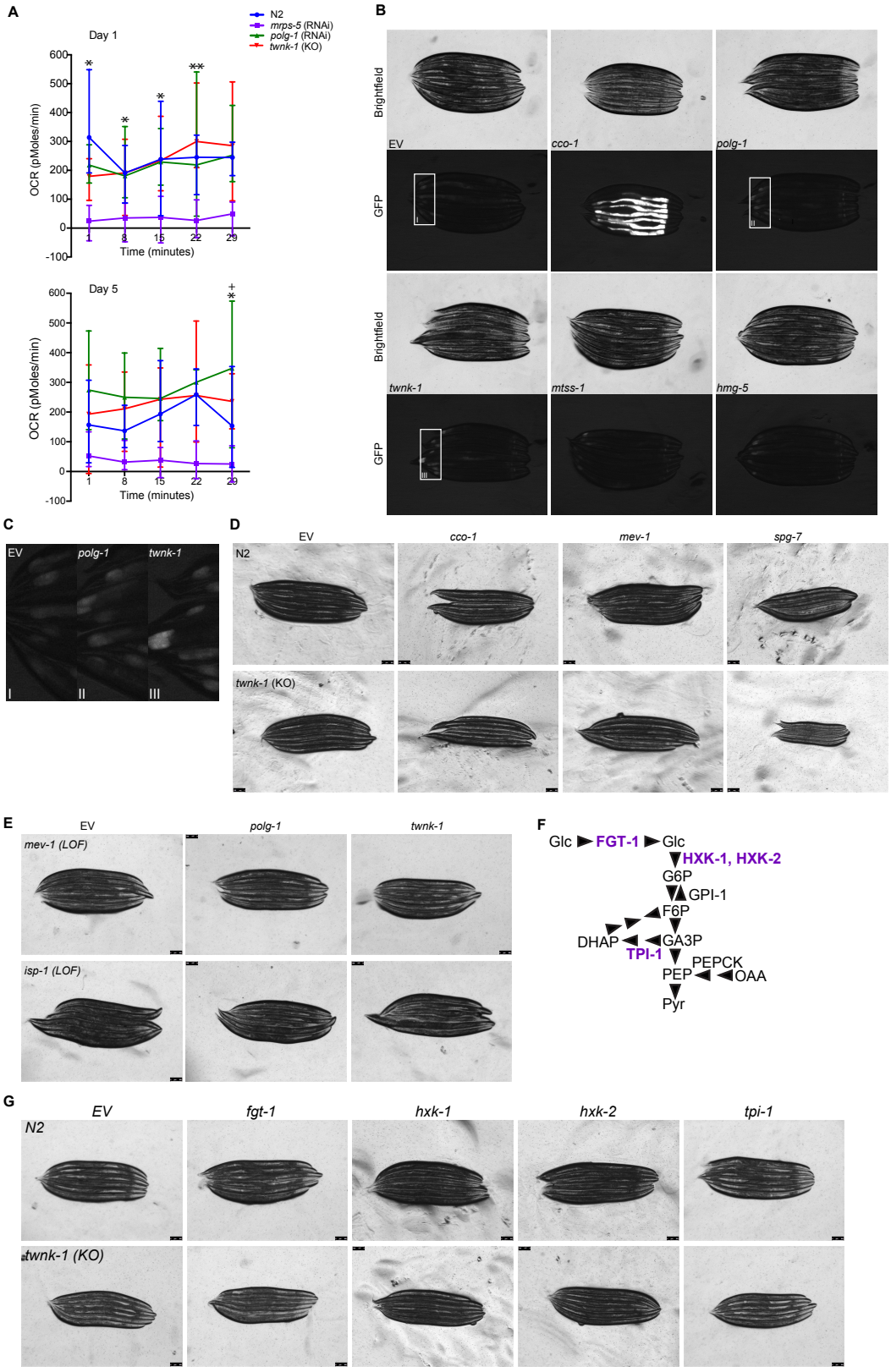

Figure 3: Loss of *twnk-1* causes no gross defects in mitochondrial function. (A) *Mutation of twnk-1 does not affect oxygen consumption rate (OCR):* OCR in *twnk-1* and control *C. elegans* lines was measured using Seahorse XFe96 Analyzer. *mrps-5* was used as a control. Results shown as mean ± SEM. Significance of *twnk-1* relative to age-matched EV animals indicated as follows: $***$ $p < 0.001$, $**p < 0.01$, $*p < 0.05$; ns, $p > 0.05$. Significance of *polg-1* (RNAi) relative to age-matched EV animals at the same time point is indicated as follows: +++ $p < 0.001$, ++$p < 0.01$, +$p < 0.05$; ns, $p > 0.05$. Changes in *mrps-5* (RNAi) OCR were significant for nearly every point. (B) *Knockdown of twnk-1 causes a subtle induction of the mitochondrial unfolded protein response (UPR^{mt}):* Activation of the UPR^{mt} reporter *hsp-6p*::GFP upon RNAi knockdown of replisome components and *hmg-5*. Zoom of hindgut knock down of *polg-1* and *twnk-1*, showing slight upregulation of the *hsp-6p*::GFP reporter in (C). (D) *Synthetic interactions with mitochondrial genes: twnk-1* and wild type control animals were grown on ETC component (*cco-1*, *mev-1*) and mitochondrial protease (*spg-7*) RNAi. The converse experiment, where ETC mutant animals (*isp-1*, *mev-1*) were grown on replisome RNAi is shown in (E). (F) *Glycolysis flow diagram:* the metabolic pathway from glucose (Glc) to pyruvate (Pyr) is depicted. Glucose transport protein 1 (FGT-1) and the enzymes hexokinase 1 (HXK-1),hexokinase 2 (HXK-2), and triosephosphate isomerase (TPI-1) are highlighted in purple, and knocked-down in wild type and *twnk-1* animals in (G).

Figure 4: Loss of *twnk-1* causes changes in mitochondrial morphology.

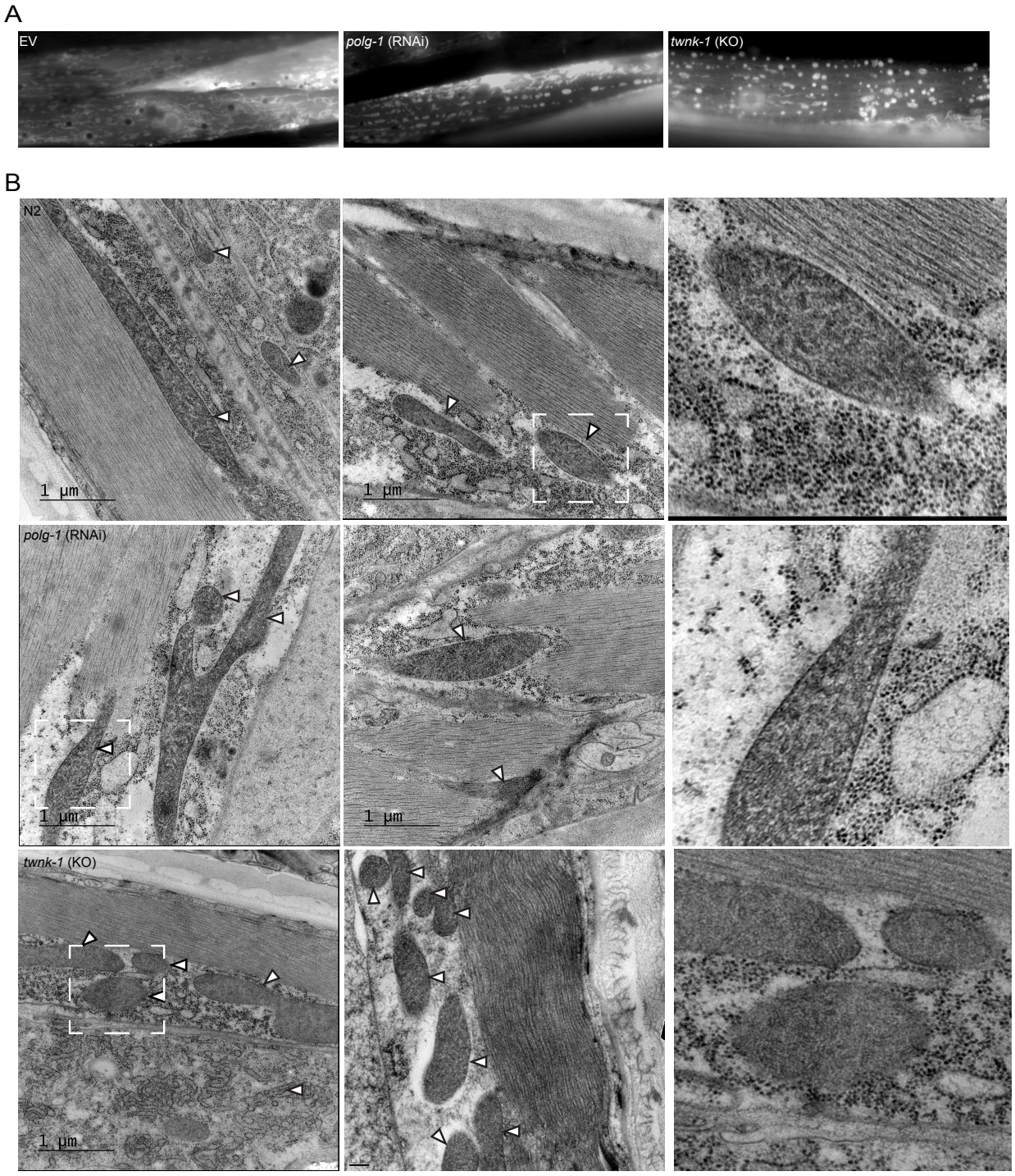

Figure 4: Loss of *twnk-1* causes changes in mitochondrial morphology. (A) *Mutation in twnk-1 causes mitochondrial fragmentation:* Fluorescent imaging of the mitochondrial network in myocytes using GFP targeted to the mitochondria as a mitochondrial marker. Wild-type animals on empty vector (EV) or *polg-1* (RNAi), and *twnk-1* mutant animals were used. (B) *Christae structure appears unperturbed with loss of twnk-1 and polg-1:* Electron micrographs of *twnk-1*, *polg-1* (RNAi), and wild-type animals. White arrows point to mitochondria. Images on the right panel are zooms of the corresponding box as indicated by dashed lines.

Figure 5: Mutation in *twnk-1* does not impair development, but reduces fecundity.

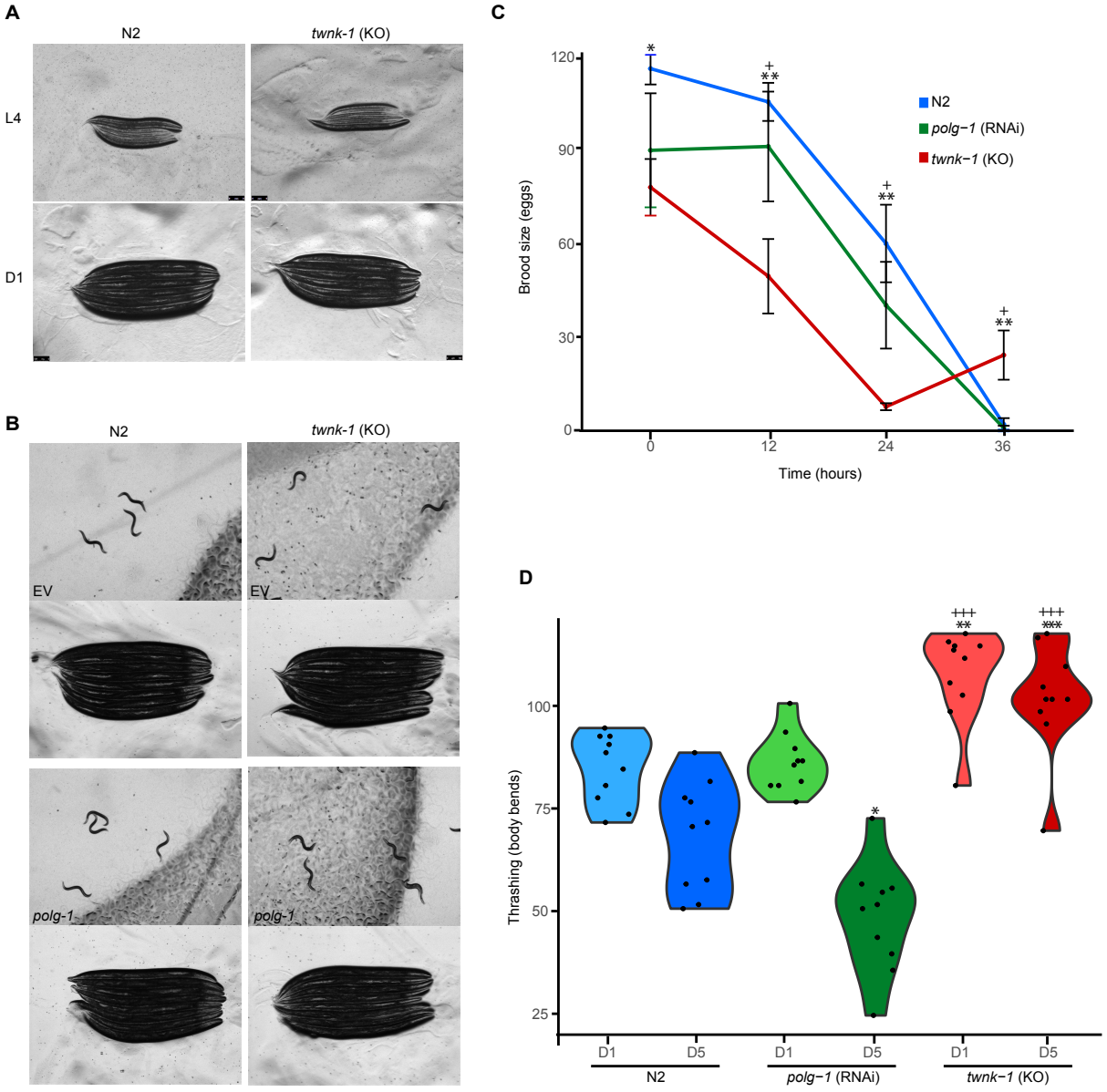

Figure 5: Mutation in *twnk-1* does not impair development, but reduces fecundity. (A) *twnk-1 mutants develop normally: twnk-1 and wild type animals were imaged at age-matched time points in L4 and D1*. Note that the development of worms was concurrent. (B) *twnk-1 mutants do not exhibit synthetic effect with polg-1 knockdown*: *twnk-1* and wild type control animals grown on *polg-1* RNAi were imaged. Low magnification pictures show the presence of eggs, indicating that the animals are fertile. (C) *Mutation in twnk-1 reduces fecundity:* Fecundity was assayed by brood size as counted by the number of eggs laid over time for wild type, *polg-1*

(RNAi), and *twnk-1* animals. Results shown as mean ± SEM. Significance of twnk-1 relative to N2 at the same time point is indicated as follows: $**p < 0.01$, $*p < 0.05$; ns, $p > 0.05$. Significance of *twnk-1* relative to *polg-1* at the same time point is indicated as follows: $+p < 0.05$; ns, $p > 0.05$. (D) *Animals mutant for twnk-1 increase thrashing:* Motility of wild type, *polg-1* (RNAi), and *twnk-1* animals, as measured by body bends (thrashing) in liquid during early and mid-adulthood. Thrashing measurements were taken over 25 seconds. Significance of *twnk-1* relative to age-matched N2 animals is indicated as follows: $*** p < 0.001$, $**p < 0.01$, $*p < 0.05$; ns, $p > 0.05$. Significance of *twnk-1* relative to *polg-1* at the same time point is indicated as follows:$+++p < 0.001$,$++p < 0.01$,$+p < 0.05$; ns, $p > 0.05$.

Figure 6: Screening alternative replicative helicases.

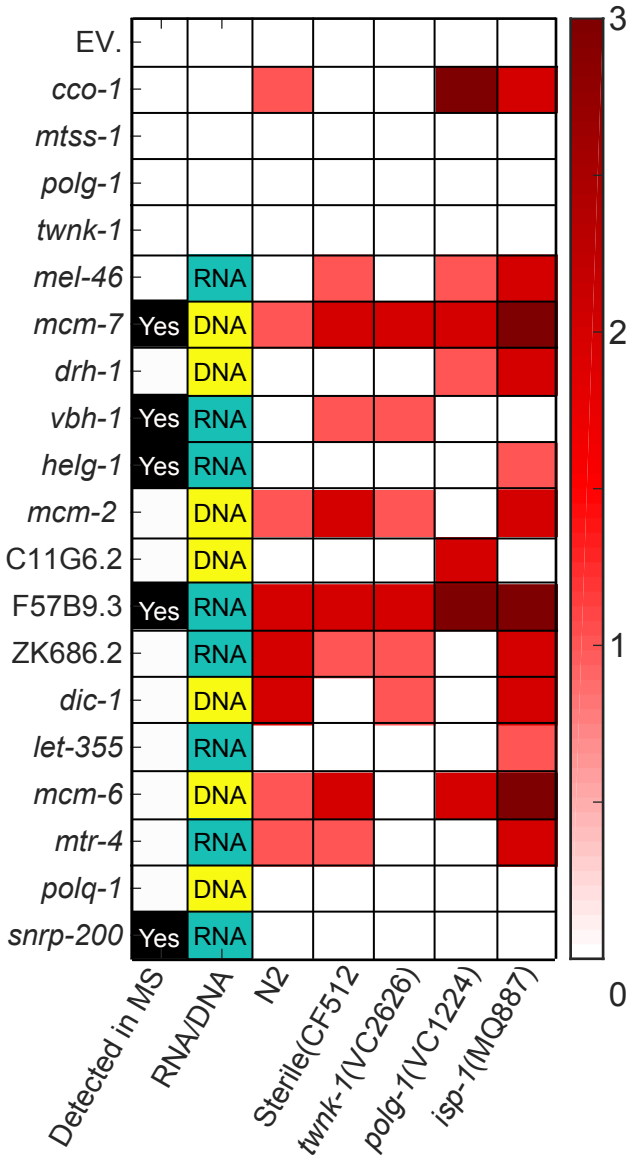

Figure 6: Screening alternative replicative helicases. A summary of the hits from the preliminary screen indicates their features: (i) detection in mass spectrometry of isolated mitochondria (ii) predicted nucleic acid type interacting with the protein, and score (from 0 to 3) for a developmental delay, arrest, and sterility as assessed by microscopy in different genetic backgrounds (iii-vii). See full table of screen results in Table S1.

Supplementary Figure 1: Schematics of mtDNA replisome and *twnk-1* locus mutation.

A

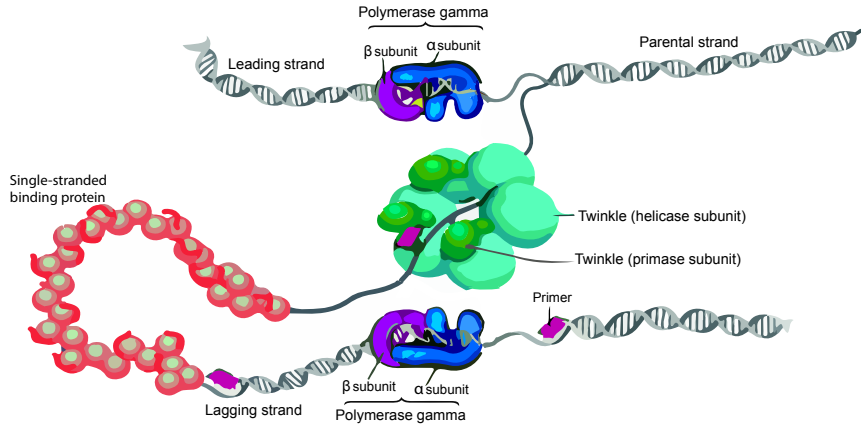

B

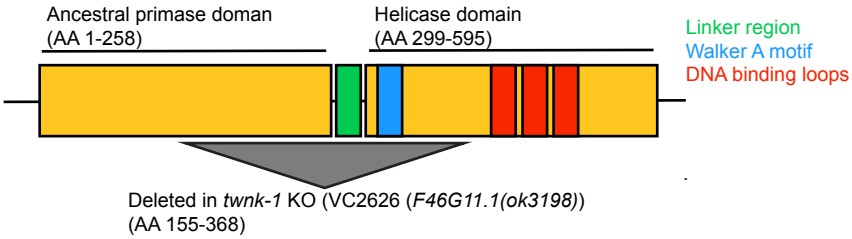

Supplementary Figure 1: Schematics of mtDNA replisome and *twnk-1* locus mutation. (A) *Schematic of the minimal mitochondrial DNA replisome in characterized metazoans.* (B) *Schematic of twnk-1 locus in wild type versus twnk-1 mutant.*

Supplementary Figure 2: *twnk-1* adults are not sensitized to UV stress.

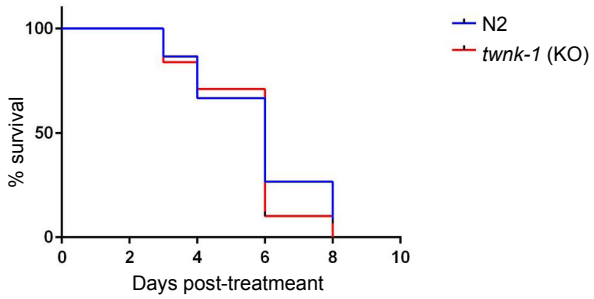

Supplementary Figure 2: *twnk-1* adults are not sensitized to UV stress. Survival curve of adult wild type versus *twnk-1* mutants after UV treatment.

Supplementary Figure 3: *twnk-1* does not decrease OCR, but does cause subtle activation of the UPR^{mt}.

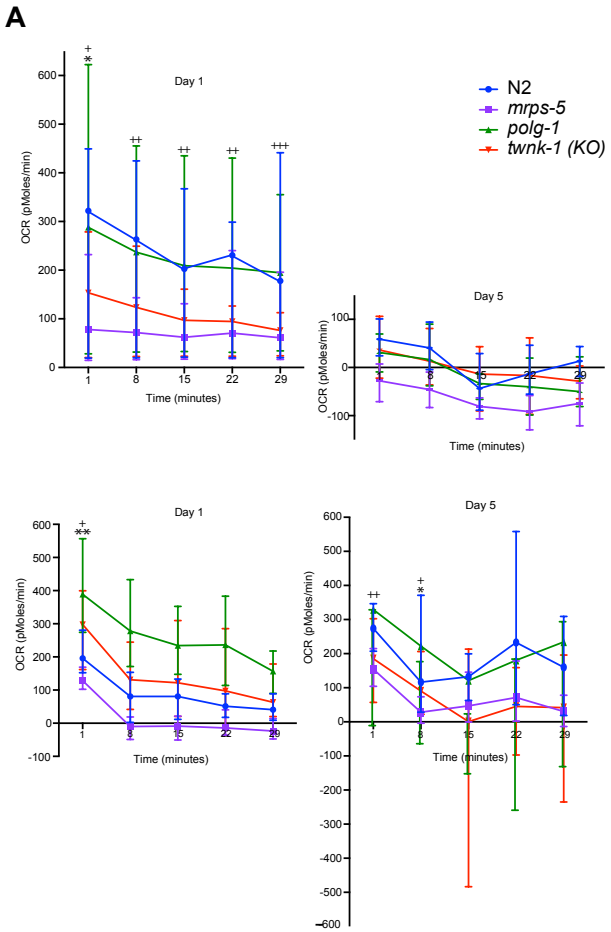

Supplementary Figure 3: *twnk-1* does not decrease OCR, but does cause subtle activation of the UPR^{mt}. (A) *Mutation of twnk-1 does not affect oxygen consumption rate (OCR)*: OCR in *twnk-1*, *polg-1* (RNAi), and control *C. elegans* lines was measured using Seahorse XFe96 Analyzer. Two independent replicates are shown here; results shown as mean ± SEM. Significance of *twnk-1* relative to wild type indicated by: $***$ $p < 0.001$, $**p < 0.01$, $*p < 0.05$; ns, $p > 0.05$. Significance of *polg-1* relative to wild type indicated by: +++ $p < 0.001$, ++$p < 0.01$, +$p < 0.05$; ns, $p > 0.05$. (B) *Two generations of RNAi knock down of twnk-1 causes a subtle induction of the mitochondrial unfolded protein response (UPR^{mt}):* Activation of the UPR^{mt} reporter *hsp-6p*::GFP upon two generations of RNAi knockdown of replisome components and *hmg-5*.

Supplementary Figure 4: Animals mutant for *twnk-1* show increased thrashing.

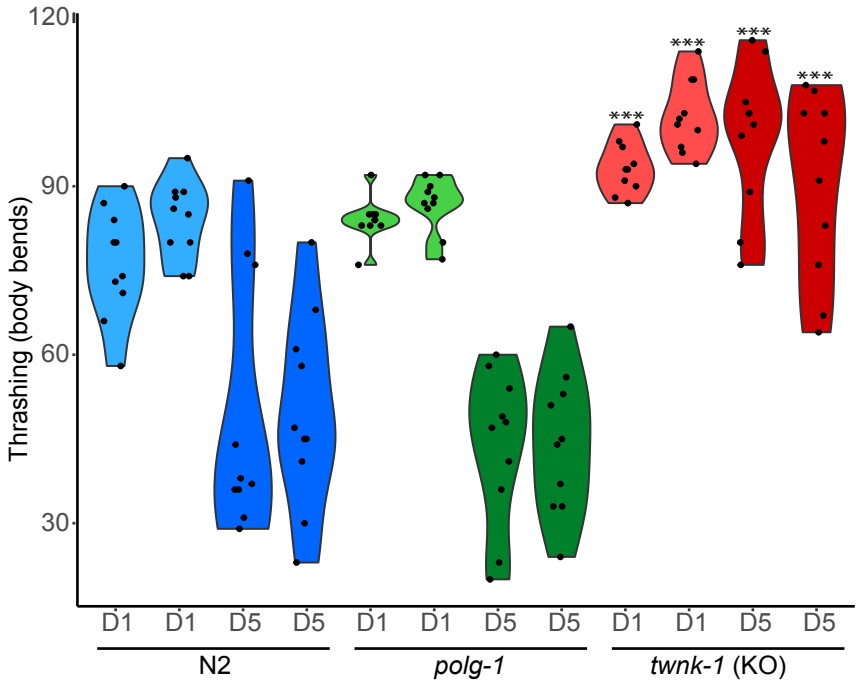

Supplementary Figure 4: Animals mutant for *twnk-1* show increased thrashing. Motility of wild type, *polg-1* (RNAi), and *twnk-1* animals, as measured by body bend (thrashing) in liquid during early and mid-adulthood. Two independent replicates are shown here. Results shown as mean ± SEM; significance relative to age-matched N2 animals shown as $***p < 0.001$,$**p < 0.01$,$*p < 0.05$; ns, $p > 0.05$. Supplementary Table 1: Complete Results of screen for alternate mtDNA replicative helicase. Indicated are gene name or locus, predicted nucleic acid type interacting with the protein, and score (from 0 to 3) for a developmental delay, arrest, and sterility as assessed by microscopy in different genetic backgrounds (iii-vii).

Supplemental Table 1: Complete Results of screen for alternate mtDNA replicative helicase. Indicated are gene name or locus, predicted nucleic acid type interacting with the protein, and score (from 0 to 3) for a developmental delay, arrest, and sterility as assessed by microscopy in different genetic backgrounds (iii-vii).

Gene Name or Locus	**N2 phenotype**	**Sperm-deficient sterile (CF512) phenotype**	***twnk-1* (VC2626) Phenotype**	***polg-1* (VC1224) phenotype**	***isp-1* (MQ887) phenotype**
empty vector (EV, plasmid L4440)	WT	Sterile eggs	WT	Reduced fertility	Delayed
cco-1	Delayed, reduced fertility	Delayed, no eggs	Delayed, reduced progeny	L4 arrest	Sterile
mtss-1	WT	Sterile eggs	WT	Reduced fertility	Delayed
polg-1	WT	Sterile eggs	WT	Reduced fertility	Delayed
twnk-1	WT	Sterile eggs	WT	Reduced fertility	Delayed
glh-2	WT	WT (related to strain on EV)	WT (related to strain on EV)	WT (related to strain on EV)	WT (related to strain on EV)
H20J04.4b	Delayed and reduced fertil	WT	very reduced fertility	Sterile	Delayed, sterile
smgl-2	WT	WT	WT	WT	Delayed, reduced fertility
F52G3.3	WT	WT	WT	WT	Delayed, reduced fertility
F19B2.5	WT	WT	WT	WT	Delayed fertility
hel-1	Larval arrest	WT	L3 arrest, some dead at D2, prot vulva	Larval arrest	Larval arrest
Y54G11A.3	WT	WT	WT	WT	Delayed
mel-46	WT	Reduced egg production	WT	Reduced fertility	Delayed, reduced fertility
mcm-7	Delayed fertility	Protruding vulva, very reduced egg production	Some animals show developemental delay, reduced progeny	Sterile	Variable penetrance larval arrest, sterile
mut-14	WT	WT	WT	WT	Delayed fertility
smut-1	WT	WT	WT	WT	Delayed fertility
tofu-2	WT	WT	WT	WT	WT
C44H9.4	WT	WT	WT	WT	Delayed fertility
skih-2	WT	WT	WT	WT	WT
psa-4	WT	WT	WT	WT	WT
mog-1	WT	WT	WT	WT	WT
chl-1	WT	WT	WT	WT	Delayed
F53H1.1	WT	WT	WT	WT	Variable penetrance larval arrest, sterile
drh-2	WT	WT	WT	WT	Delayed fertility
drh-1	WT	WT	WT	Reduced fertility	Variable penetrance larval arrest, delayed fertility
vbh-1	WT	Reduced egg production	some dead adults at D2	Reduced movement	Delayed fertility
helg-1	WT	WT	WT	Sterile	Delayed fertility
F52B5.3	WT	WT	WT	WT	WT
F11C3.1	WT	WT	WT	WT	Delayed fertility
C24H12.4a	WT	WT	WT	WT	Reduced body size
ZK250.9	WT	WT	WT	WT	Reduced body size
btf-1	Delayed, sterile	WT	Variable penetrance larval arrest, sterile	L4 arrest	Reduced body size
C28H8.3	WT	WT	WT	WT	Delayed
MCM-2	Delayed fertility	No egg production	Delayed fertility	Sterile, protruding vulva	WT
Y113G7B.14	WT	WT	WT	WT	Reduced fertility
chd-3	WT	WT	WT	WT	WT
C11G6.2	WT	WT	WT	Reduced movement	WT
rde-12	WT	WT	WT	WT	Reduced fertility
M04C3.2	WT	WT	WT	WT	Delayed
C25F9.5	WT	WT	WT	WT	Delayed
dcr-1	WT	WT	WT	WT	Variable penetrance larval arrest, sterile
rha-2	Delayed and reduced fertility	WT	Very reduced fertility	Delayed, sterile	Variable penetrance larval arrest, sterile
T26G10.1	Delayed, sterile	WT	Very reduced fertility, protruding vulva	Variable penetrance larval arrest, sterile	Reduced body size, sterile
C16A3.1	WT	WT	WT	WT	Delayed
F57B9.3	Delayed, sterile	Variable penetrance larval arrest, reduced egg production	Variable penetrance larval arrest, sterile	Larval arrest	Larval arrest
wrn-1	Variable penetrance larval arrest, sterile	WT	Variable penetrance larval arrest, sterile	Larval arrest	Larval arrest
ZK686.2	Variable penetrance larval arrest, sterile	Reduced egg production	Very reduced fertility	Sterile	Delayed, sterile
ddx-23	Very reduced fertility	WT	Very reduced fertility	Variable penetrance larval arrest, sterile	Reduced fertility, second gen sterile
ddx-19	WT	WT	WT	WT	Delayed
rha-1	WT	WT	WT	WT	Reduced fertility
Y54E2A.4	WT	WT	WT	WT	Delayed
chd-1	WT	WT	WT	WT	Delayed
glh-1	WT	WT	WT	WT	WT
drh-3	WT	WT	WT	WT	Delayed
dog-1	WT	WT	WT	WT	Delayed
dic-1	Reduced fertility	WT	reduced progeny	Sterile	Delayed, sterile
let-355	WT	WT	WT	Reduced fertility	Delayed, reduced fertility
mcm-6	Delayed fertility	Variable penetrance larval death	Delayed fertility	Delayed, sterile	Variable penetrance larval arrest, sterile
mtr-4	Delayed fertility	Reduced egg production	WT	Variable penetrance larval arrest, sterile	Variable penetrance larval arrest
R03D7.2	WT	WT	WT	WT	WT
cku-80	WT	WT	WT	WT	WT
xnp-1	WT	WT	WT	WT	WT
glh-3	WT	WT	WT	WT	WT
cgh-1	WT	WT	WT	WT	WT

mcm-3	WT	WT	WT	WT	WT
C25F9.4	WT	WT	WT	WT	WT
rad-26	WT	WT	WT	WT	Delayed
eri-1	Dead at D2	WT	WT	WT	WT
rcq-5	Larval death	WT	Variable penetrance larval arrest, sterile	Larval arrest	Larval arrest
mog-5	WT	WT	WT	WT	WT
bch-1	WT	WT	WT	WT	WT
let-418	WT	WT	WT	WT	WT
F33D11.10	WT	WT	WT	WT	WT
csb-1	WT	WT	WT	WT	WT
ddx-15	WT	WT	WT	WT	WT
inf-1	WT	WT	WT	WT	WT
ddx-17	WT	WT	WT	WT	WT
sacy-1	WT	WT	WT	WT	WT
M03C11.8	WT	WT	WT	WT	WT
M04C3.1	WT	WT	WT	WT	WT
mcm-5	Delayed and reduced fertil	WT	Very reduced fertility	Reduced fertility	Sterile
him-6	WT	WT	WT	WT	Delayed
chd-7	WT	WT	WT	WT	WT
T05A12.4	Dead at D2	WT	WT	WT	WT
glh-4	WT	WT	WT	WT	Variable penetrance larval arrest, sterile
T23H2.3	WT	WT	WT	WT	WT
polq-1	WT	WT	WT	Reduced fertility	WT
rad-54	WT	WT	WT	WT	WT
Y116A8C.13	WT	WT	WT	WT	Delayed
fbxc-55	WT	WT	WT	WT	Delayed fertility
mcm-4	WT	WT	WT	WT	WT
Y116A8C.13	WT	WT	WT	WT	WT
snrp-200	WT	WT	WT	Reduced fertility	WT
cku-70	WT	WT	WT	WT	WT
smg-2	WT	WT	WT	WT	WT
xpd-1	WT	WT	WT	WT	WT
helq-1	WT	WT	WT	WT	WT
cec-8	Delayed, reduced fertility	WT	WT	WT	Delayed
Y65B4A.6	devp delayed a day, reduced body size	WT	some L4 arrested, some YA, reduced fertility	WT	Larval arrest
xpb-1	WT	WT	WT	WT	WT
ddx-35	WT	WT	WT	WT	WT
ddx-27	WT	WT	WT	WT	WT
laf-1	WT	WT	WT	WT	WT
emb-4	WT	WT	WT	WT	WT
Y94H6A.5a	WT	WT	WT	WT	WT
ZK1067.2	WT	WT	WT	WT	WT
ZK512.2	WT	WT	WT	WT	WT
F54E12.2	WT	WT	WT	WT	WT
F59A7.8	WT	WT	WT	WT	WT
C52B9.8	WT	WT	WT	WT	WT
ruvb-2	Sterile	WT	Sterile	Sterile	Sterile
ddx-19	WT	WT	Sterile	WT	WT
C08F8.2	WT	WT	WT	WT	Sterile
C05C10.2	WT	WT	WT	WT	WT
dna-2	WT	WT	WT	WT	WT
let-765	Reduced fertility	WT	Sterile	Sterile	Sterile
Y50D7A.11	Reduced fertility	WT	Sterile	Sterile	Sterile
ruvb-1	Sterile	WT	Sterile	Sterile	Sterile
ssl-1	WT	WT	WT	WT	WT
R05D11.4	WT	WT	WT	WT	WT
mog-4	Sterile	WT	Larval arrest	Sterile	Larval arrest
F55F8.2	Reduced fertility	WT	Sterile	Sterile	Sterile
B0511.6	Sterile	WT	Sterile	Sterile	Larval arrest
pif-1	WT	WT	WT	WT	WT
Y55F3BR.1	WT	WT	Sterile	WT	WT
C46F11.4	WT	WT	WT	WT	WT
F33H12.6	WT	WT	WT	WT	WT
Y116F11A.1	WT	WT	WT	WT	WT
F59H6.5	WT	WT	WT	WT	WT

Chapter 4: Glia signal the mitochondrial unfolded protein response to distal tissues

4.1 Introduction

Cells orchestrate and coordinate a number of different stress-response mechanisms in response to various perturbations. Different subcellular compartments are able to monitor the health of their proteins, and respond to proteostatic challenges by initiating stress responses. Over the last decade and a half, our lab and others have shown that stressors sometimes actually extend the lifespan of an organism. This is thought to be due to the protective effects of activating these stress responses a dynamic known as hormesis. Indeed, genetic induction of stress responses in the absence of stressors has the same effect, supporting this hypothesis (20,21,104–106).

In this project, I focused on the UPR^{mt}, a genetic program that is activated upon challenges to mitochondrial health. This response works to decrease global protein translation while simultaneously increasing production of mitochondrial chaperones and proteases that work to restore mitochondrial protein homeostasis (124,130,131). Cells throughout an organism autonomously activate this quality control mechanism in response to stress. Additionally, our lab has shown that when neurons are subject to mitochondrial stress that activates the UPR^{mt}, they activate the UPR^{mt} in distal tissues in a cell non-autonomous manner. This tissue-specific stress and non-autonomous signaling is sufficient to increase the organism's lifespan (20,21,26,27). Our lab has also shown that the homolog of the chromatin modifier PHF8, *jmjd-1.2* in worms, is a necessary component of UPR^{mt} signaling. Jmjd-1.2/PHF8 is histone demethylase of 2-oxoglutarate dependent oxygenase that works on a range of substrates: H3K9me1/2, H3K27me2 and H4K20me1(132–136). It is associated with upregulation of gene expression and the removal of repressive marks, perhaps playing a role in the upregulation of stress-responsive genes. Overexpression of *jmjd-1.2a* in neurons is sufficient to induce distal UPR^{mt} activation and extend organismal lifespan (21).

In addition to neurons, the nervous system contains glia cells. *C. elegans* glia most closely resemble vertebrate astrocytes, a glial subtype that is abundant in the mammalian CNS. Recent advances in the field of glial biology show that astrocytes are highly secretory; important in memory, learning, and synaptic plasticity(76,77,79,137); and can signal between themselves in a calcium-dependent manner (72,138). In *C. elegans*, glia have been shown to be crucial to axon guidance and morphology (88,95) and sensory organ function (90), and modulates dopamine-dependent behaviors (139) and sleep (91). Glia are currently defined by four promoters: *mir-228* (pan-glial), *fig-1* (amphid sheath glia), *ptr-10* (most glia, excepting amphid sheath glia), and *hlh-17* (cephalic sheath glia) (68,87,88,95).

In forthcoming work, our lab shows that glia are capable of transmitting organelle stress (UPR^{ER}) to distal tissues, turning on the UPR^{ER} in a cell-nonautonomous manner. This extends

lifespan even more robustly than neuronal signaling of the UPR^{ER} (101 and Frakes et al, forthcoming in *Cell*). Inspired by this work, we hypothesized that glia may also be able to signal the UPR^{mt} to distal tissues. We investigated glial signaling in the context of the UPR^{mt}. We examined the ability of a subset of glia to signal the UPR^{mt} non-autonomously, the effects of signaling on lifespan and stress resistance, and the molecular mechanisms behind this signaling. This work is ongoing, and will be completed by my colleagues Dr. Raz Bar-Ziv and Samira Monshietehadi after I graduate.

4.2 Results

Glia signal the UPR^{mt} to distal tissues

Previous work from our lab has shown that expressing the key UPR^{mt} component histone demethylase *jmjd-1.2a* under the neuron-specific promoter *rgef-1* is sufficient to induce UPR^{mt} in distal tissues in *C. elegans* (21). To assay if glia can signal the UPR^{mt} to distal tissues, we attempted to express *jmjd-1.2a* under the four known glia promoters. We were unable to make animals expressing this gene under the pan-glial *mir-228* promoter or under the amphid sheath glia *fig-1* promoter, even when injecting these constructs at very low concentrations and with a variety of injection markers. We were able to make animals with an extrachromosomal array expressing *jmjd-1.2a* under the promoter *ptr-10*, which is expressed in most glia cells, excepting amphid sheath (AMsh) glia. Monitoring activation of the UPR^{mt} by looking at transcription of the canonical UPR^{mt} chaperone *hsp-6* using animals expressing *hsp-6p::*GFP, we saw subtle activation of the UPR^{mt} with mixed penetrance in lines with the *ptr-10p::jmjd-1.2a* array. In addition to weak UPR^{mt} activation, these animals has no extension in lifespan, so we did not study them further (Fig S1).

Animals expressing *jmjd-1.2a* under the cephalic sheath (CEPsh) glia promoter *hlh-17* showed activation of the aforementioned *hsp-6p*::GFP UPR^{mt} reporter (Fig 1A). *hlh-17* is a homolog of the mammalian gene Olig that is required for normal response to dopamine signaling (139), and is specific to CEPsh glia in *C. elegans* (95). Specifically, we saw activation of the UPR^{mt} in the intestine. This induction was dependent on the canonical UPR^{mt} transcription factor ATFS-1. ATFS-1 is an unusual transcription factor has both a mitochondrial signal sequence and nuclear localization sequence. In non-stressed conditions, it accumulates in mitochondria, where it is degraded. Under stressed conditions, perhaps because membrane potential and therefore import capability are reduced in compromised mitochondria, it is imported into the nucleus, where it activates stress-response genes (17,18). Additionally, *hlh-17p::jmjd-1.2a* did not induce the endoplasmic reticulum unfolded protein response (UPR^{ER}) or the heat shock response (HSR) (Fig 1C). While we generated three independent integrated strains expressing *hlh-17p::jmjd-1.2a*, which all showed UPR^{mt} activation, we chose to focus the majority of our studies on one of these lines, as the two others had mating defects and were prone to multivulva phenotype.

We looked for *hsp-6p*::GFP signal in the CEPsh glia of *hlh-17p::jmjd-1.2a* animals, comparing high magnifcation of nerve ring and amphid sensillum region to these areas in the *hlh-17p*::GFP promoter reporter, but did not see evidence of UPR^{mt} activation in these cells (data not shown). We attempted to quantify the stress response by qPCR measuring mRNA levels of the canonical UPR^{mt} chaperones *hsp-6* and *hsp-60*, as well as primers against canonical chaperones of the UPR^{ER} and the HSR. However, results were inconsistent (data not shown). Indeed, previous work from our lab has shown that induction of chaperones of these stress

pathways as measured by qPCR is subtle at best. Thus, to quantify the stress response, we used a COPAS Biosorter to measure flouresence down the length of the animal (Fig 1B). This preliminary quantification shows that the expression of hsp-6p::GFP in *hlh-17p::jmjd-1.2a* animals is significant relative to the background expression of GFP in the reporter strain. This difference was pronounced in the hindgut.

We validated these results using a second reporter for the UPR^{mt}. When the UPR^{mt} is activated, the transcription factor DVE-1 translocates from the cytoplasm to the nucleus (15,20). Using transgenic animals expressing a *dve-1p::dve-1*::GFP to track the location of DVE-1, we saw nuclear localization of the reporter in intestinal nuclei upon CEPsh glia expression of *jmjd-1.2a* (Fig 2A). Nuclear localization was strongly suppressed by RNAi against *lin-65*, which previous work from our lab has shown to be coregulated with DVE-1 (20). Interestingly, this localization was not suppressed by RNAi against *atfs-1*. These results support previous work suggesting that DVE-1, LIN-65, and MET-2 work together, while ATFS-1 works as a separate signalling branch of the UPR^{mt}(20) (Fig 2B). We also examined the effect of RNAi treatment against *met-2* and *ubl-5*. Ubl-5 RNAi may cause subtle suppression; we are currently quantitating the DVE-1 data.

The genetic overexpression of *jmjd-1.2a* assays the ability of glia cells to transmit a mitochondrial stress signal once it is activated within the cells. It does not directly speak to the ability of these cells to sense endogenous mitochondrial stress. To more directly address this question, we attempted to make animals expressing mitochondria-targeted KillerRed, a red flourescent protein that generates reactive oxygen species. Previous worked showed that expression of KillerRed in neurons was sufficient to induce a cell non-autonomous UPR^{mt} (28). Unfotunately, we were unable to make animals expressing KillerRed under the *hlh-17* promoter, even when injecting the construct with different coinjection markers and at a very low concentration. We hope to explore this question by using a hairpin targeting electron transport chain component *cco-1* in glia (26).

Glia induction of the UPR^{mt} increases lifespan and stress resistance

Because glial expression of *jmjd-1.2a* induced a non-autonomous UPR^{mt} signal, we hypothesized that lifespan would be extended in these animals, as in neuronal UPR^{mt} induction by *jmjd-1.2a* overexpresssion. Indeed, we saw increased lifespan in all three independent integrant strains of *hlh-17p::jmjd-1.2a* (Fig 3A-C). We used *atfs-1* as a control for UPR^{mt} contribution to lifespan, but found it caused a mild reduction in wild type lifespan and did not effecively suppressed glial *jmjd-1.2a* lifespan extension.

As a further test of the physiological effects of glial UPR^{mt} induction, we assayed the ability of *hlh-17p*::*jmjd-1.2a* animals to withstand paraquat, a chemical stressor that generates reactive oxygen species which disproportionately target mitochondria. A preliminary lifespan experiment on paraquat showed that these already long-lived animals lived even longer when subject to a low-level, on-going paraquat stress (Fig 3D). We followed up this intriguing finding with more classic acute paraquat stress assays. In these assays, glial *jmjd-12.a* animals had similar paraquat resistance to our positive control, *daf-2* RNAi (140) (Fig 3E), indicative of an increased capacity to withstand mitochondrial stress.

4.3 Discussion

Our work has shown that glia are capable of sending signals to distal tissues, adding to the growing body of evidence that glia are involved in complex brain functions, perhaps even information processing (72,141,142). We found that expressing the UPR^{mt} component and signal-inducer *jmjd-1.2a* in four CEPsh glia by using the *hlh-17* promoter induced the UPR^{mt} in distal tissues, as measured by fluorescent signal from the transcriptional reporter *hsp-6p*::GFP. We quantified this result, and confirmed it with an additional reporter which shows nucear localization of DVE-1 induced by the UPR^{mt}. These results were dependent on different known UPR^{mt} components: *hsp-6p*::GFP signal was dependent on *atfs-1*, while the localization of *dve-1p::dve-1*::GFP to nuclei was independent of *atfs-1*, but dependent on *lin-65*. This supports previous work in the lab that suggests there are two distinct signaling branches of the UPR^{mt}.

Glial activation of the UPR^{mt} extends lifespan, and increases resistance to the acute mitochondrial stress induced by paraquat treatment. These results suggest that activation of the UPR^{mt} by glia is physiologically meaningful, preserving and even buttressing mitochondrial health. Together, these exciting results add to the growing body of evidence that glia cells are not mere "glue" as their name suggests, but that they have critical roles in information processing, signaling, and organismal health.

At the time of publication of this thesis, this work is ongoing. I am quantitating DVE-1 reporter localization under glial UPR^{mt} signalling. My colleagues are in the process of replicating the *hsp-6p*::GFP reporter data. We are also in the process of repeated lifespan assays.

In a model of mitochondrial stress induced by an expansion of glutamates, the causitive molecular pathology in Huntington's Disease, our lab found that the communication of neuronal stress to distal tissues was dependent on the release of dense core vessicles, which rely on expression of the gene *unc-31* (27). DCVs transport neuropeptides, and are one of two main chemical signalling mechanisms used by neurons. The other is small clear vessicles (SVCs), which rely on the expression of *unc-13* to transport neurotransmitters and biogenic amines (143). To learn more about the molecular mechanisms of glial UPR^{mt} signaling, we are curretnly examining both UPR*mt* reporters in the context of mutations in *unc-13* and *unc-31*. In the aforementioned polyglutamate work, serotonin was a critical signal component. We are also looking at stress reporters under glial *jmjd-1.2a* overexpression in the context of mutation of *tph-1*, a serotonin production gene.

4.4 Figures

Figure 1: Glia signal the UPR^{mt} to distal tissues in *C. elegans*.

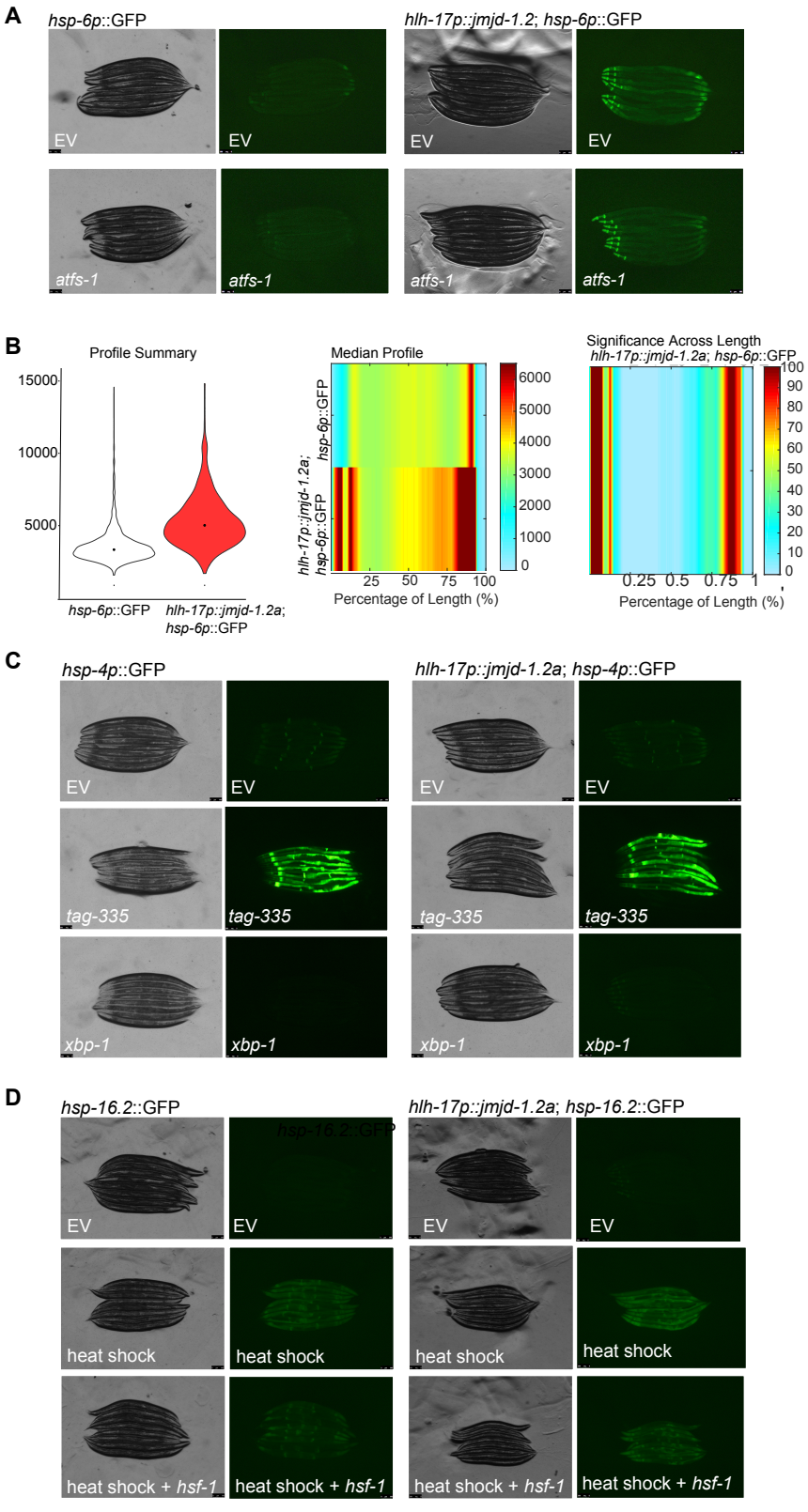

Figure 1: Glia signal the UPR^{mt} to distal tissues in *C. elegans*. (A) *Overexpression of jmjd-1.2a in CEPsh glia activates the UPR^{mt} in distal tissues*. Fluorescence in the pharynx is channel bleed through from the tdTomato transgene marker. (B) *Whole animal sorting using the COPAS Biosorter quantifies fluorescence down the length of the animal*. Violin plot shows whole animal fluorescence on the y-axis. Middle image shows the median profile for worms of each strain, with animals aligned left (anterior) to right (posterior) in arbitrary units of fluorescence. Difference in anterior region is due to bleed over from the tdTomato transgenic marker in the pharynx. Image on the right shows significance plots. "$-1.3\text{-}\log_{10}$(*P-value*)" was plotted which distinguished regions of significance by Wilcoxon Rank Sum Test (113). A value ≥ 0 is equivalent to $P \leq 0.05$; the difference in green fluorescence between the reporter strain (*hsp-6p*::GFP) and the experimental strain (hlh-*17p::jmjd-1.2a*; *hsp-6p*::GFP) was significant, especially in the hindgut. (C) *hlh-17p::jmjd-1.2a overexpression does not induce the UPR^{ER} or HSR*.

Figure 2: Glia UPR^{mt} causes nuclear localization of DVE-1 in an *atfs-1* independent manner.

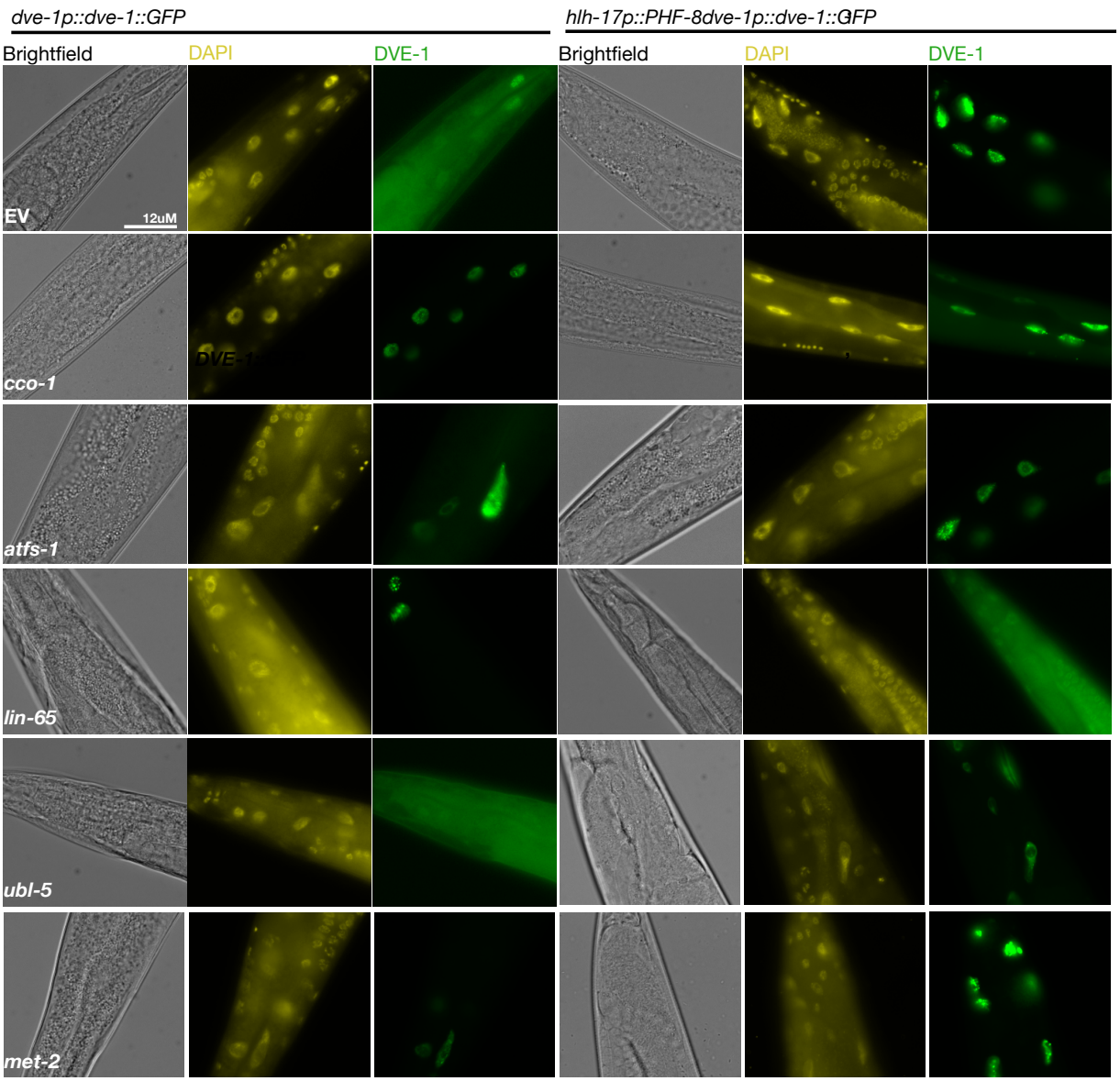

Figure 2: Glia UPR^{mt} causes nuclear localization of DVE-1 in an atfs-1 independent manner. (A) *Glial expression of jmjd-1.2a causes nuclear localization of a DVE-1 reporter*. Image shown is hindgut. DAPI was used to confirm identity of intestinal nuclei. This effect is strongly suppressed by *lin-65* RNAi, and partially suppressed by *ubl-5* RNAi. This effect does not seem to be suppressed by RNAi against *atfs-1*.

Figure 3: Glial activation of the UPR^{mt} extends lifespan and increases oxidative stress resistant.

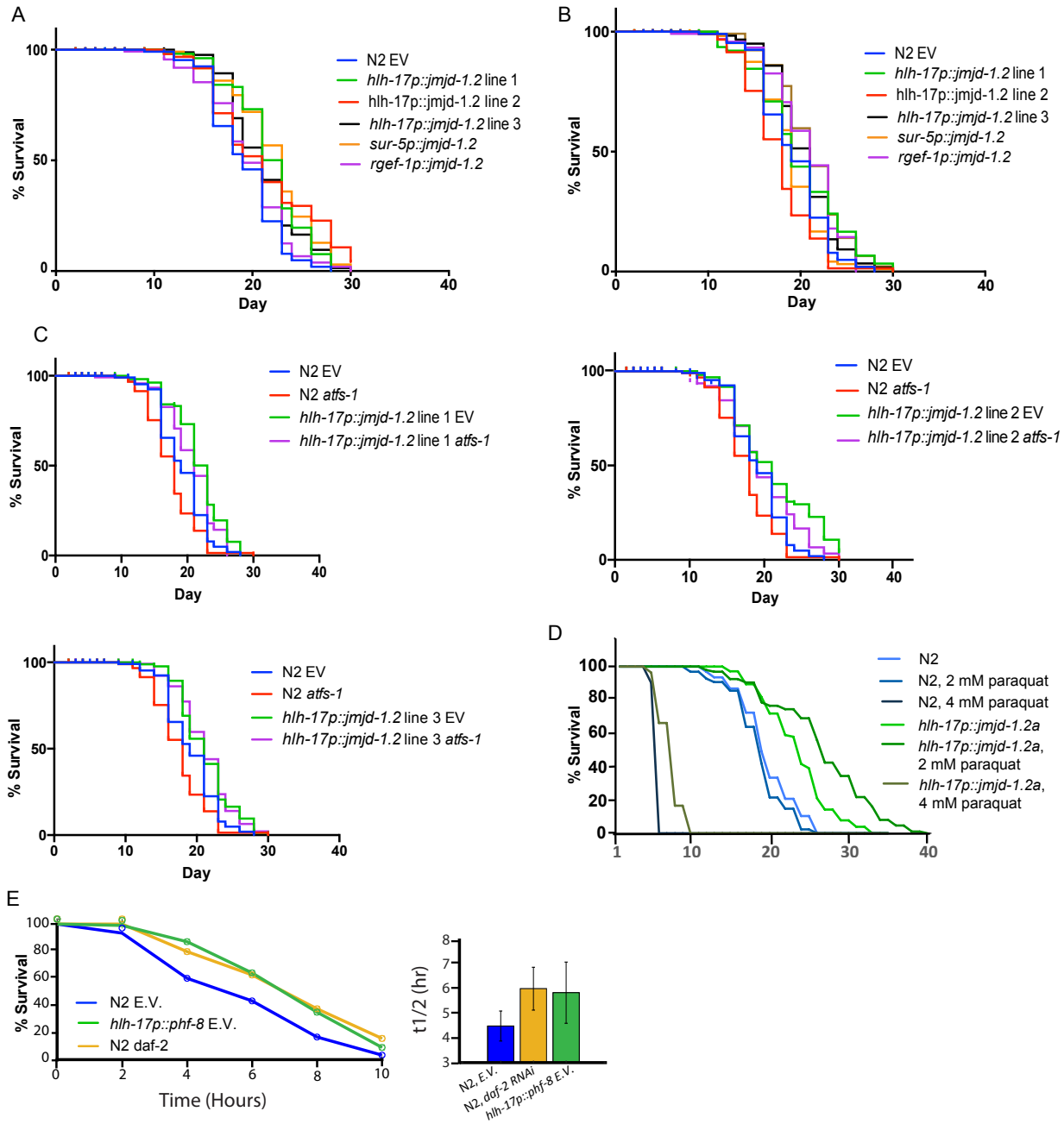

Figure 3: Glial activation of the UPR^{mt} extends lifespan and increases oxidative stress resistant. (A) *Lifespan of wild type (N2) animals, animals expressing neuronal jmjd-1.2a under the rgef-1 promoter, animals expressing jmjd-1.2a under the intestinal promoter gly-19, and three independent integrant strains of hlh-17p::jmjd-1.2a on empty vector RNAi.* (B) *Lifespan of the same strains on atfs-1 RNAi.* (C) *Lifespan of each hlh-17p::jmjd-1.2a strain versus N2 on EV versus atfs-1 RNAi, separating for ease of viewing.*

Supplementary Figure 1: Glial expression of *jmjd-1.2* by the *ptr-10* promoter does not extend lifespan.

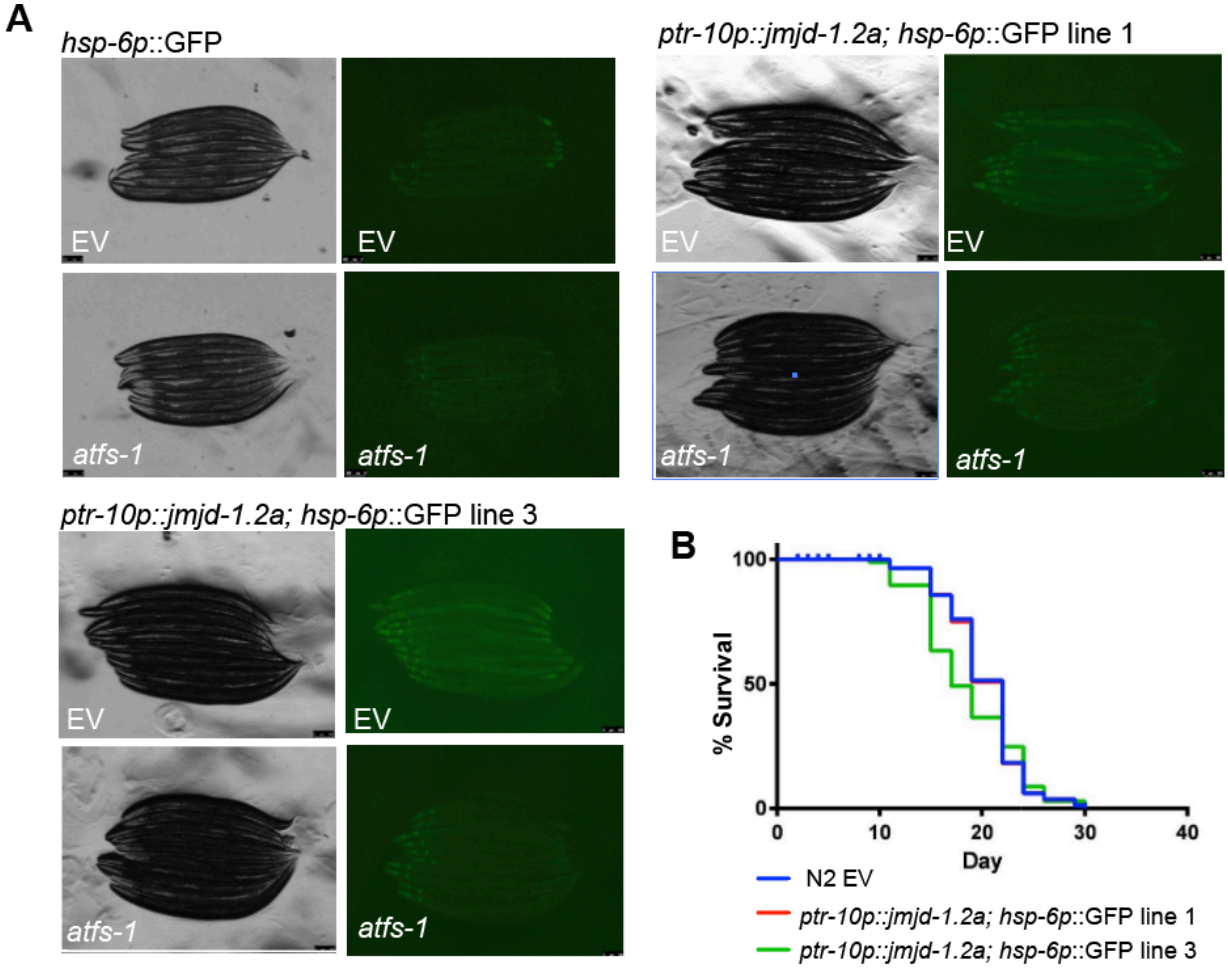

Supplementary Figure 1: Glial expression of *jmjd-1.2* by the ptr-10 promoter does not extend lifespan. (A) *Overexpression of ptr-10p::jmj-1.2a causes slight upregulation of the UPR*^{mt}. (B) *Overexpression of ptr-10p::jmj-1.2a does not extend lifespan*.

Chapter 5: Conclusions and Future Directions

5.1 Conclusions and future directions

Our work on the function of TWNK-1 in *C. elegans* yielded surprising results: despite being the sole homolog of the mtDNA replicative helicase Twinkle, *twnk-1* is not necessary for mtDNA replication or maintenance in this organism. We have shown that lack of *twnk-1* does, however, affect mitochondrial function: larval animals have decreased resistance to UV stress and starvation, *twnk-1* RNAi induces the UPR^{mt}, loss of *twnk-1* causes synthetic arrest with knockdown of the mitochondrial protease spg-7, and loss of *twnk-1* causes mitochondrial fragmentation, a classic indicator of mitochondrial stress.

Further efforts for this work would ideally take two paths: 1) finding a required mtDNA replicative helicase in *C. elegans* and 2) making a PEO disease model using mutation in *polg-1*. The first step to finding the helicase is completing the RNAi screen by making RNAi clones of the helicases not available/sequence-verified from the available RNAi libraries. A more in-depth screening method, though laborious, might include screening for loss of mtDNA content under helicase RNAi treatment in *twnk-1* mutant animals, as it is possible that TWNK-1 and another mtDNA replicative helicase are functioning redundantly.

For the goal of making a PEO disease model, I would turn to *polg-1*. Mutations in PolG are also known to cause PEO, and some of these are small mutations in areas with high sequence conservation in *C. elegans*. The CRISPR-Cas system would be ideal for inducing these mutations. If we were able to create stable lines, the next steps would be to do metabolic analysis to further understand the molecular basis of the syndrome, RNAi screening to find genetic modulators, and screening small molecules to find possible drug treatments to slow progress of the disease.

Our work on glial signaling of the UPRmt has yielded exciting results: CEPsh glia cells can signal the UPR^{mt} to distal tissues in *C. elegans*. This signaling is physiologically significant: animals with glial activation of UPR^{mt} by overexpression of *jmjd-1.2a* are long-lived. They are also resistant to paraquat, which creates damaging reactive oxygen species in mitochondria. Our results add to a growing body of work uncovering the many important roles of glia cells, particularly astrocyte and astrocyte-like glia.

Work on glial UPR^{mt} signaling is ongoing as of this publication. We are repeating and quantifying a number of assays, including UPR^{mt} activation with two reporters and lifespan assays. Finally, we are use mutations in neural signaling pathways to further understand how glia signal the UPR^{mt} to distal tissues. Our results add to a growing body of work uncovering the many important roles of glia cells, particularly astrocyte and astrocyte-like glia.

Chapter 6: References

1. Gorman GS, Chinnery PF, DiMauro S, Hirano M, Koga Y, McFarland R, et al. Mitochondrial diseases. Nat Rev Dis Prim [Internet]. 2016;2:16080. Available from: http://www.ncbi.nlm.nih.gov/pubmed/27775730
2. Friedman JR, Nunnari J. Mitochondrial form and function. Nature [Internet]. 2014 Jan 16;505(7483):335–43. Available from: http://www.ncbi.nlm.nih.gov/pubmed/24429632
3. Chacinska A, Koehler CM, Milenkovic D, Lithgow T, Pfanner N. Importing mitochondrial proteins: machineries and mechanisms. Cell [Internet]. 2009 Aug 21;138(4):628–44. Available from: http://www.ncbi.nlm.nih.gov/pubmed/19703392
4. Pagliarini DJ, Calvo SE, Chang B, Sheth SA, Vafai SB, Ong S-E, et al. A mitochondrial protein compendium elucidates complex I disease biology. Cell [Internet]. 2008 Jul 11;134(1):112–23. Available from: http://www.ncbi.nlm.nih.gov/pubmed/18614015
5. Katharine B, Yufei L, Danica C. Aging: The Mitochondrial Connection. J Clin Exp Pathol. 2012;s4(01).
6. Nicholls DG. Mitochondrial membrane potential and aging. Aging Cell. 2004.
7. Ichishita R, Tanaka K, Sugiura Y, Sayano T, Mihara K, Oka T. An RNAi Screen for Mitochondrial Proteins Required to Maintain the Morphology of the Organelle in Caenorhabditis elegans. J Biochem [Internet]. 2008 Apr;143(4):449–54. Available from: https://academic.oup.com/jb/article-lookup/doi/10.1093/jb/mvm245
8. Chaudhari SN, Kipreos ET. Increased mitochondrial fusion allows the survival of older animals in diverse C. Elegans longevity pathways. Nat Commun. 2017;
9. Palikaras K, Lionaki E, Tavernarakis N. Coordination of mitophagy and mitochondrial biogenesis during ageing in C. elegans. Nature. 2015;
10. Sugiura A, McLelland G-L, Fon EA, McBride HM. A new pathway for mitochondrial quality control: mitochondrial-derived vesicles. EMBO J [Internet]. 2014 Oct 1;33(19):2142–56. Available from: http://www.ncbi.nlm.nih.gov/pubmed/25107473
11. Cadete VJJ, Deschênes S, Cuillerier A, Brisebois F, Sugiura A, Vincent A, et al. Formation of mitochondrial-derived vesicles is an active and physiologically relevant mitochondrial quality control process in the cardiac system. J Physiol [Internet]. 2016;594(18):5343–62. Available from: http://www.ncbi.nlm.nih.gov/pubmed/27311616
12. Laberge R-M, Adler D, DeMaria M, Mechtouf N, Teachenor R, Cardin GB, et al. Mitochondrial DNA damage induces apoptosis in senescent cells. Cell Death Dis [Internet]. 2013 Jul 18;4(7):e727–e727. Available from: http://www.nature.com/articles/cddis2013199
13. Singh KK. Mitochondria damage checkpoint in apoptosis and genome stability. FEMS Yeast Res [Internet]. 2004 Nov;5(2):127–32. Available from: http://www.ncbi.nlm.nih.gov/pubmed/15489195
14. Xie L, Zhu X, Hu Y, Li T, Gao Y, Shi Y, et al. Mitochondrial DNA Oxidative Damage Triggering Mitochondrial Dysfunction and Apoptosis in High Glucose-Induced HRECs. Investig Opthalmology Vis Sci [Internet]. 2008 Sep 1;49(9):4203. Available from: http://iovs.arvojournals.org/article.aspx?doi=10.1167/iovs.07-1364
15. Haynes CM, Petrova K, Benedetti C, Yang Y, Ron D. ClpP Mediates Activation of a Mitochondrial Unfolded Protein Response in C. elegans. Dev Cell. 2007;
16. Haynes CM, Yang Y, Blais SP, Neubert TA, Ron D. The matrix peptide exporter HAF-1

signals a mitochondrial UPR by activating the transcription factor ZC376.7 in C. elegans. Mol Cell [Internet]. 2010 Feb 26;37(4):529–40. Available from: http://www.ncbi.nlm.nih.gov/pubmed/20188671
17. Nargund AM, Pellegrino MW, Fiorese CJ, Baker BM, Haynes CM. Mitochondrial import efficiency of ATFS-1 regulates mitochondrial UPR activation. Science (80-). 2012;
18. Nargund AM, Fiorese CJ, Pellegrino MW, Deng P, Haynes CM. Mitochondrial and nuclear accumulation of the transcription factor ATFS-1 promotes OXPHOS recovery during the UPR(mt). Mol Cell [Internet]. 2015 Apr 2;58(1):123–33. Available from: http://www.ncbi.nlm.nih.gov/pubmed/25773600
19. Benedetti C, Haynes CM, Yang Y, Harding HP, Ron D. Ubiquitin-like protein 5 positively regulates chaperone gene expression in the mitochondrial unfolded protein response. Genetics. 2006;
20. Tian Y, Garcia G, Bian Q, Steffen KK, Joe L, Wolff S, et al. Mitochondrial Stress Induces Chromatin Reorganization to Promote Longevity and {UPR(mt).}. Cell. 2016;165(5):1197–208.
21. Merkwirth C, Jovaisaite V, Durieux J, Matilainen O, Jordan SD, Quiros PM, et al. Two Conserved Histone Demethylases Regulate Mitochondrial {Stress-Induced} Longevity. Cell. 2016;165(5):1209–23.
22. Fiorese CJ, Schulz AM, Lin YF, Rosin N, Pellegrino MW, Haynes CM. The Transcription Factor ATF5 Mediates a Mammalian Mitochondrial UPR. Curr Biol. 2016;
23. Lehtonen JM, Forsström S, Bottani E, Viscomi C, Baris OR, Isoniemi H, et al. {FGF21} is a biomarker for mitochondrial translation and {mtDNA} maintenance disorders. Neurology. 2016;87(22):2290–9.
24. Tyynismaa H, Carroll C, Raimundo N, Sofia A-E, Wenz T, Ruhanen H, et al. Mitochondrial myopathy induces a starvation-like response. Hum Mol Genet. 2010;19(20):3948–58.
25. Tyynismaa H, Carroll CJ, Raimundo N, Ahola-Erkkilä S, Wenz T, Ruhanen H, et al. Mitochondrial myopathy induces a starvation-like response. Hum Mol Genet [Internet]. 2010 Oct 15;19(20):3948–58. Available from: http://www.ncbi.nlm.nih.gov/pubmed/20656789
26. Durieux J, Wolff S, Dillin A. The cell-non-autonomous nature of electron transport chain-mediated longevity. Cell [Internet]. 2011 Jan 7;144(1):79–91. Available from: http://www.ncbi.nlm.nih.gov/pubmed/21215371
27. Berendzen KM, Durieux J, Shao L-WW, Tian Y, Kim H-EE, Wolff S, et al. Neuroendocrine Coordination of Mitochondrial Stress Signaling and Proteostasis. Cell [Internet]. 2016 Sep 8;166(6):1553–1563.e10. Available from: http://www.ncbi.nlm.nih.gov/pubmed/27610575
28. Shao L-WW, Niu R, Liu Y. Neuropeptide signals cell non-autonomous mitochondrial unfolded protein response. Cell Res. 2016;26(11):1182–96.
29. Li C, Kim K. Neuropeptides in Wormbook. In: Wormbook. 2005.
30. Nunnari J, Suomalainen A. Mitochondria: In Sickness and in Health. Cell. 2012;148(6):1145–59.
31. Goffart S, Cooper HM, Tyynismaa H, Wanrooij S, Suomalainen A, Spelbrink JN. Twinkle mutations associated with autosomal dominant progressive external ophthalmoplegia lead to impaired helicase function and in vivo {mtDNA} replication stalling. Hum Mol Genet. 2008;18(2):328–40.

32. Tyynismaa H, Sembongi H, Bokori-Brown M, Granycome C, Ashley N, Poulton J, et al. Twinkle helicase is essential for mtDNA maintenance and regulates mtDNA copy number. Hum Mol Genet. 2004;13(24):3219–27.
33. Tyynismaa H, Mjosund KP, Wanrooij S, Lappalainen I, Ylikallio E, Jalanko A, et al. Mutant mitochondrial helicase Twinkle causes multiple {mtDNA} deletions and a late-onset mitochondrial disease in mice. Proc Natl Acad Sci {USA}. 2005;102(49):17687–92.
34. Goethem G, Martin J-J, Broeckhoven C. Progressive External Ophthalmoplegia Characterized by Multiple Deletions of Mitochondrial {DNA:} Unraveling the Pathogenesis of Human Mitochondrial {DNA} Instability and the Initiation of a Genetic Classification. Neuromol Med. 2003;3(3):129–46.
35. Lönnqvist T. Infantile-Onset Spinocerebellar Ataxia [Internet]. GeneReviews®. 2009. Available from: http://www.ncbi.nlm.nih.gov/pubmed/20301746
36. Nikali K, Suomalainen A, Saharinen J, Kuokkanen M, Spelbrink JN, Lönnqvist T, et al. Infantile onset spinocerebellar ataxia is caused by recessive mutations in mitochondrial proteins Twinkle and Twinky. Hum Mol Genet [Internet]. 2005 Oct 15;14(20):2981–90. Available from: http://www.ncbi.nlm.nih.gov/pubmed/16135556
37. Hakonen AH, Isohanni P, Paetau A, Herva R, Suomalainen A, Lönnqvist T. Recessive Twinkle mutations in early onset encephalopathy with mtDNA depletion. Brain [Internet]. 2007 Nov;130(Pt 11):3032–40. Available from: http://www.ncbi.nlm.nih.gov/pubmed/17921179
38. Korhonen JA, Pham XH, Pellegrini M, Falkenberg M. Reconstitution of a minimal mtDNA replisome in vitro. EMBO J [Internet]. 2004 Jun 16;23(12):2423–9. Available from: http://www.ncbi.nlm.nih.gov/pubmed/15167897
39. Wanrooij S, Falkenberg M. The human mitochondrial replication fork in health and disease. Biochim Biophys Acta [Internet]. 2010 Aug;1797(8):1378–88. Available from: http://www.ncbi.nlm.nih.gov/pubmed/20417176
40. Spelbrink JN, Li FY, Tiranti V, Nikali K, Yuan QP, Tariq M, et al. Human mitochondrial DNA deletions associated with mutations in the gene encoding Twinkle, a phage T7 gene 4-like protein localized in mitochondria. Nat Genet. 2001;28(3):223–31.
41. Shutt TE, Gray MW. Twinkle, the mitochondrial replicative DNA helicase, is widespread in the eukaryotic radiation and may also be the mitochondrial DNA primase in most eukaryotes. J Mol Evol [Internet]. 2006 May;62(5):588–99. Available from: http://www.ncbi.nlm.nih.gov/pubmed/16612544
42. Fernández-Millán P, Lázaro M, Cansız-Arda Ş, Gerhold JM, Rajala N, Schmitz C-A, et al. The hexameric structure of the human mitochondrial replicative helicase Twinkle. Nucleic Acids Res [Internet]. 2015 Apr 30;43(8):4284–95. Available from: http://www.ncbi.nlm.nih.gov/pubmed/25824949
43. Holmlund T, Farge G, Pande V, Korhonen J, Nilsson L, Falkenberg M. Structure–function defects of the twinkle amino-terminal region in progressive external ophthalmoplegia. Biochim Biophys Acta - Mol Basis Dis [Internet]. 2009 Feb;1792(2):132–9. Available from: https://linkinghub.elsevier.com/retrieve/pii/S0925443908002287
44. Peter B, Farge G, Pardo-Hernandez C, Tångefjord S, Falkenberg M. Structural basis for adPEO-causing mutations in the mitochondrial TWINKLE helicase. Hum Mol Genet [Internet]. 2019 Apr 1;28(7):1090–9. Available from: http://www.ncbi.nlm.nih.gov/pubmed/30496414
45. Kaguni LS, Oliveira MT. Structure, function and evolution of the animal mitochondrial

replicative DNA helicase. Crit Rev Biochem Mol Biol [Internet]. 2016;51(1):53–64. Available from: http://www.ncbi.nlm.nih.gov/pubmed/26615986
46. Nunnari J, Suomalainen A. Mitochondria: In sickness and in health. Cell [Internet]. 2012;148(6):1145–59. Available from: http://dx.doi.org/10.1016/j.cell.2012.02.035
47. Martin-Negrier M-L, Sole G, Jardel C, Vital C, Ferrer X, Vital A. TWINKLE gene mutation: report of a French family with an autosomal dominant progressive external ophthalmoplegia and literature review. Eur J Neurol [Internet]. 2011 Mar;18(3):436–41. Available from: http://www.ncbi.nlm.nih.gov/pubmed/20880070
48. Suomalainen A, Majander A, Wallin M, Setälä K, Kontula K, Leinonen H, et al. Autosomal dominant progressive external ophthalmoplegia with multiple deletions of mtDNA: clinical, biochemical, and molecular genetic features of the 10q-linked disease. Neurology [Internet]. 1997 May;48(5):1244–53. Available from: http://www.ncbi.nlm.nih.gov/pubmed/9153451
49. Tyynismaa H, Mjosund KP, Wanrooij S, Lappalainen I, Ylikallio E, Jalanko A, et al. Mutant mitochondrial helicase Twinkle causes multiple mtDNA deletions and a late-onset mitochondrial disease in mice. Proc Natl Acad Sci U S A [Internet]. 2005 Dec 6;102(49):17687–92. Available from: http://www.ncbi.nlm.nih.gov/pubmed/16301523
50. Nikkanen J, Forsström S, Euro L, Paetau I, Kohnz RA, Wang L, et al. Mitochondrial {DNA} Replication Defects Disturb Cellular {dNTP} Pools and Remodel {One-Carbon} Metabolism. Cell Metab. 2016;23(4):635–48.
51. Baqri RM, Turner BA, Rheuben MB, Hammond BD, Kaguni LS, Miller KE. Disruption of mitochondrial DNA replication in Drosophila increases mitochondrial fast axonal transport in vivo. PLoS One [Internet]. 2009 Nov 17;4(11):e7874. Available from: http://www.ncbi.nlm.nih.gov/pubmed/19924234
52. Bratic A, Kauppila TES, Macao B, Grönke S, Siibak T, Stewart JB, et al. Complementation between polymerase- and exonuclease-deficient mitochondrial DNA polymerase mutants in genomically engineered flies. Nat Commun [Internet]. 2015 Nov 10;6:8808. Available from: http://www.ncbi.nlm.nih.gov/pubmed/26554610
53. Williams AJ, Kaguni LS. Stimulation of Drosophila mitochondrial DNA polymerase by single-stranded DNA-binding protein. J Biol Chem [Internet]. 1995 Jan 13;270(2):860–5. Available from: http://www.ncbi.nlm.nih.gov/pubmed/7822323
54. Thömmes P, Farr CL, Marton RF, Kaguni LS, Cotterill S. Mitochondrial single-stranded DNA-binding protein from Drosophila embryos. Physical and biochemical characterization. J Biol Chem [Internet]. 1995 Sep 8;270(36):21137–43. Available from: http://www.ncbi.nlm.nih.gov/pubmed/7673145
55. Maier D, Farr CL, Poeck B, Alahari A, Vogel M, Fischer S, et al. Mitochondrial single-stranded DNA-binding protein is required for mitochondrial DNA replication and development in Drosophila melanogaster. Mol Biol Cell [Internet]. 2001 Apr;12(4):821–30. Available from: http://www.ncbi.nlm.nih.gov/pubmed/11294889
56. Bratic I, Hench J, Henriksson J, Antebi A, Bürglin TR, Trifunovic A. Mitochondrial {DNA} level, but not active replicase, is essential for Caenorhabditis elegans development. Nucleic Acids Res. 2009;37(6):1817–28.
57. Addo M, Cossard R, Pichard D, Kwasi O-D, Rötig A, Delahodde A. Caenorhabditis elegans, a pluricellular model organism to screen new genes involved in mitochondrial genome maintenance. Biochim Biophys Acta Bba - Mol Basis Dis. 2010;1802(9):765–73.
58. Tsang WY, Lemire BD. Mitochondrial Genome Content Is Regulated during Nematode

Development. Biochem Bioph Res Co. 2002;291(1):8–16.
59. Bratic I, Hench J, Trifunovic A. Caenorhabditis elegans as a model system for mtDNA replication defects. Methods [Internet]. 2010 Aug;51(4):437–43. Available from: http://www.ncbi.nlm.nih.gov/pubmed/20230897
60. Stiban J, Farnum GA, Hovde SL, Kaguni LS. The N-terminal domain of the Drosophila mitochondrial replicative DNA helicase contains an iron-sulfur cluster and binds DNA. J Biol Chem [Internet]. 2014 Aug 29;289(35):24032–42. Available from: http://www.ncbi.nlm.nih.gov/pubmed/25023283
61. Sanchez-Martinez A, Calleja M, Peralta S, Matsushima Y, Hernandez-Sierra R, Whitworth AJ, et al. Modeling Pathogenic Mutations of Human Twinkle in Drosophila Suggests an Apoptosis Role in Response to Mitochondrial Defects. PLoS One. 2012;7(8):1–11.
62. Eki T, Ishihara T, Katsura I, Hanaoka F. A Genome-wide Survey and Systematic {RNAi-based} Characterization of Helicase-like Genes in Caenorhabditis elegans. Dna Res. 2007;14(4):183–99.
63. Lemire B. Mitochondrial genetics. WormBook [Internet]. 2005 Sep 14;1–10. Available from: http://www.ncbi.nlm.nih.gov/pubmed/18023115
64. Tsang WY, Lemire BD. The role of mitochondria in the life of the nematode, Caenorhabditis elegans. Biochim Biophys Acta [Internet]. 2003 Jul 14;1638(2):91–105. Available from: http://www.ncbi.nlm.nih.gov/pubmed/12853115
65. Yasuda K, Ishii T, Suda H, Akatsuka A, Hartman PS, Goto S, et al. Age-related changes of mitochondrial structure and function in Caenorhabditis elegans. Mech Ageing Dev [Internet]. 2006 Oct;127(10):763–70. Available from: http://www.ncbi.nlm.nih.gov/pubmed/16893561
66. Brown K. Aging: The Mitochondrial Connection. J Clin Exp Pathol [Internet]. 2012;s4(01). Available from: https://www.omicsonline.org/aging-the-mitochondrial-connection-2161-0681.S4-003.php?aid=7328
67. Cortopassi GA, Arnheim N. Detection of a specific mitochondrial {DNA} deletion in tissues of older humans. Nucleic Acids Res. 1990;18(23):6927–33.
68. Oikonomou G, Shaham S. The glia of Caenorhabditis elegans. Glia [Internet]. 2011 Sep;59(9):1253–63. Available from: http://www.ncbi.nlm.nih.gov/pubmed/21732423
69. von Bartheld CS, Bahney J, Herculano-Houzel S. The search for true numbers of neurons and glial cells in the human brain: A review of 150 years of cell counting. Journal of Comparative Neurology. 2016.
70. Takano H, Fellin T, Dong J-H, Haydon PG, Halassa MM. Synaptic Islands Defined by the Territory of a Single Astrocyte. J Neurosci. 2007;
71. Chung WS, Clarke LE, Wang GX, Stafford BK, Sher A, Chakraborty C, et al. Astrocytes mediate synapse elimination through MEGF10 and MERTK pathways. Nature. 2013;
72. Halassa MM, Fellin T, Haydon PG. The tripartite synapse: roles for gliotransmission in health and disease. Trends Mol Med [Internet]. 2007 Feb;13(2):54–63. Available from: http://www.ncbi.nlm.nih.gov/pubmed/17207662
73. White JG, Southgate E, Thomson JN, Brenner S. The Structure of the Nervous System of the Nematode Caenorhabditis elegans. Philos Trans R Soc B Biol Sci. 2006;
74. Ullian EM, Sapperstein SK, Christopherson KS, Barres BA. Control of synapse number by glia. Science (80-). 2001;
75. Chung WS, Allen NJ, Eroglu C. Astrocytes control synapse formation, function, and

elimination. Cold Spring Harb Perspect Biol. 2015;
76. Adamsky A, Kol A, Kreisel T, Doron A, Ozeri-Engelhard N, Melcer T, et al. Astrocytic Activation Generates De Novo Neuronal Potentiation and Memory Enhancement. Cell. 2018;
77. Santello M, Toni N, Volterra A. Astrocyte function from information processing to cognition and cognitive impairment. Nat Neurosci. 2019;
78. Brockett AT, Kane GA, Monari PK, Briones BA, Vigneron PA, Barber GA, et al. Evidence supporting a role for astrocytes in the regulation of cognitive flexibility and neuronal oscillations through the Ca2+ binding protein S100β. PLoS One. 2018;
79. Navarrete M, Perea G, de Sevilla DF, Gómez-Gonzalo M, Núñez A, Martín ED, et al. Astrocytes mediate in vivo cholinergic-induced synaptic plasticity. PLoS Biol. 2012;
80. Ullian EM, Christopherson KS, Barres BA. Role for glia in synaptogenesis. GLIA. 2004.
81. Martín R, Bajo-Grañeras R, Moratalla R, Perea G, Araque A. Circuit-specific signaling in astrocyte-neuron networks in basal ganglia pathways. Science [Internet]. 2015 Aug 14;349(6249):730–4. Available from: http://www.ncbi.nlm.nih.gov/pubmed/26273054
82. Pehar M, Harlan BA, Killoy KM, Vargas MR. Role and Therapeutic Potential of Astrocytes in Amyotrophic Lateral Sclerosis. Curr Pharm Des [Internet]. 2017;23(33):5010–21. Available from: http://www.ncbi.nlm.nih.gov/pubmed/28641533
83. Birch AM, Katsouri L, Sastre M. Modulation of inflammation in transgenic models of Alzheimer's disease. Journal of Neuroinflammation. 2014.
84. Gleichman AJ, Carmichael ST. Astrocytic therapies for neuronal repair in stroke. Neuroscience Letters. 2014.
85. Devinsky O, Vezzani A, Najjar S, De Lanerolle NC, Rogawski MA. Glia and epilepsy: Excitability and inflammation. Trends in Neurosciences. 2013.
86. Wallace SW, Singhvi A, Liang Y, Lu Y, Shaham S. PROS-1/Prospero Is a Major Regulator of the Glia-Specific Secretome Controlling Sensory-Neuron Shape and Function in C. elegans. Cell Rep [Internet]. 2016 Apr 19;15(3):550–62. Available from: http://www.ncbi.nlm.nih.gov/pubmed/27068465
87. Rapti G, Li C, Shan A, Lu Y, Shaham S. Glia initiate brain assembly through noncanonical Chimaerin-Furin axon guidance in C. elegans. Nat Neurosci. 2017;20(10):1350–60.
88. Shaham S. Glial development and function in the nervous system of Caenorhabditis elegans. Cold Spring Harb Perspect Biol. 2015;
89. Singhvi A, Shaham S. Glia-Neuron Interactions in Caenorhabditis elegans. Annu Rev Neurosci [Internet]. 2019 Mar 18; Available from: http://www.ncbi.nlm.nih.gov/pubmed/30883261
90. Bacaj T, Tevlin M, Lu Y, Shaham S. Glia are essential for sensory organ function in C. elegans. Science (80-). 2008;
91. Katz M, Corson F, Iwanir S, Biron D, Shaham S. Glia Modulate a Neuronal Circuit for Locomotion Suppression during Sleep in C. elegans. Cell Rep. 2018;
92. Colón-Ramos DA, Margeta MA, Shen K. Glia promote local synaptogenesis through UNC-6 (netrin) signaling in C. elegans. Science (80-). 2007;
93. Shao Z, Watanabe S, Christensen R, Jorgensen EM, Colón-Ramos DA. Synapse location during growth depends on glia location. Cell [Internet]. 2013 Jul 18;154(2):337–50. Available from: http://www.ncbi.nlm.nih.gov/pubmed/23870123
94. Wallace SW, Singhvi A, Liang Y, Lu Y, Shaham S. PROS-1/Prospero Is a Major

Regulator of the Glia-Specific Secretome Controlling Sensory-Neuron Shape and Function in C. elegans. Cell Rep. 2016;
95. Yoshimura S, Murray JI, Lu Y, Waterston RH, Shaham S. mls-2 and vab-3 control glia development, hlh-17/Olig expression and glia-dependent neurite extension in C. elegans. Development. 2008;
96. Singhvi A, Frank CA, Garriga G. The T-box gene tbx-2, the homeobox gene egl-5 and the asymmetric cell division gene ham-1 specify neural fate in the HSN/PHB lineage. Genetics. 2008;
97. Sulston JEE, Schierenberg E, White JGG, Thomson JNN. The embryonic cell lineage of the nematode Caenorhabditis elegans. Dev Biol. 1983;
98. Bennett ML, Maniatis T, Wu JQ, Deng S, Zhang Y, O'Keeffe S, et al. An RNA-Sequencing Transcriptome and Splicing Database of Glia, Neurons, and Vascular Cells of the Cerebral Cortex. J Neurosci. 2014;
99. Mano I, Straud S, Wright T, Driscoll M. C. elegans glutamate transporters regulate neuronal inhibition, excitation, and cell death. In: International Worm Meeting. 2003.
100. Felton CM, Johnson CM. Dopamine Signaling in C. elegans Is Mediated in Part by HLH-17-Dependent Regulation of Extracellular Dopamine Levels . G3: Genes|Genomes|Genetics. 2014;
101. Ogata K, Kosaka T. Structural and quantitative analysis of astrocytes in the mouse hippocampus. Neuroscience. 2002;
102. Altun ZF, Hall DH. Worm Atlas. Wormatlas. 2009.
103. Bae Y-K, Barr MM. Sensory roles of neuronal cilia: cilia development, morphogenesis, and function in C. elegans. Front Biosci [Internet]. 2008 May 1;13:5959–74. Available from: http://www.ncbi.nlm.nih.gov/pubmed/18508635
104. Baird NA, Douglas PM, Simic MS, Grant AR, Moresco JJ, Wolff SC, et al. HSF-1-mediated cytoskeletal integrity determines thermotolerance and life span. Science [Internet]. 2014 Oct 17;346(6207):360–3. Available from: http://www.ncbi.nlm.nih.gov/pubmed/25324391
105. Douglas PM, Baird NA, Simic MS, Uhlein S, McCormick MA, Wolff SC, et al. Heterotypic Signals from Neural HSF-1 Separate Thermotolerance from Longevity. Cell Rep. 2015;
106. Taylor RC, Dillin A. XXBP-1 Is a cell-nonautonomous regulator of stress resistance and longevity. Cell. 2013;
107. Chase D, Koelle M. Genetic analysis of RGS protein function in Caenorhabditis elegans. Methods Enzymol. 2004;389:305–20.
108. Nawa M, Kage-Nakadai E, Aiso S, Okamoto K, Mitani S, Matsuoka M. Reduced expression of BTBD10, an Akt activator, leads to motor neuron death. Cell Death Differ. 2012;
109. Lin Y-F, Schulz AM, Pellegrino MW, Lu Y, Shaham S, Haynes CM. Maintenance and propagation of a deleterious mitochondrial genome by the mitochondrial unfolded protein response. 2016;533(7603):nature17989.
110. Chen ATY, Guo C, Itani OA, Budaitis BG, Williams TW, Hopkins CE, et al. Longevity genes revealed by integrative analysis of isoform-specific daf-16/FoxO mutants of caenorhabditis elegans. Genetics. 2015;
111. Bess AS, Crocker TL, Ryde IT, Meyer JN. Mitochondrial dynamics and autophagy aid in removal of persistent mitochondrial {DNA} damage in Caenorhabditis elegans. Nucleic

Acids Res. 2012;40(16):7916–31.
112. Hall DH, Hartwieg E, Nguyen KCQ. Modern Electron Microscopy Methods for C. elegans. Methods Cell Biol. 2012;
113. Daniele JR, Esping DJ, Garcia G, Parsons LS, Arriaga EA, Dillin A. "High-Throughput Characterization of Region-Specific Mitochondrial Function and Morphology". Sci Rep [Internet]. 2017;7(1):6749. Available from: http://www.ncbi.nlm.nih.gov/pubmed/28751733
114. Dillin A. Timing Requirements for Insulin/IGF-1 Signaling in C. elegans. Science (80-) [Internet]. 2002 Oct 25;298(5594):830–4. Available from: http://www.sciencemag.org/cgi/doi/10.1126/science.1074240
115. Young MJ, Copeland WC. Human mitochondrial DNA replication machinery and disease. Curr Opin Genet Dev [Internet]. 2016;38(1):52–62. Available from: http://www.ncbi.nlm.nih.gov/pubmed/22176657
116. Ylikallio E, Tyynismaa H, Tsutsui H, Ide T, Suomalainen A. High mitochondrial DNA copy number has detrimental effects in mice. Hum Mol Genet [Internet]. 2010 Jul 1;19(13):2695–705. Available from: http://www.ncbi.nlm.nih.gov/pubmed/20413656
117. Tyynismaa H, Suomalainen A. Mouse models of mitochondrial DNA defects and their relevance for human disease. EMBO Rep [Internet]. 2009 Feb;10(2):137–43. Available from: http://www.ncbi.nlm.nih.gov/pubmed/19148224
118. Matsushima Y, Kaguni LS. Differential phenotypes of active site and human autosomal dominant progressive external ophthalmoplegia mutations in Drosophila mitochondrial DNA helicase expressed in Schneider cells. J Biol Chem. 2007;282(13):9436–44.
119. Ciesielski GL, Nadalutti CA, Oliveira MT, Jacobs HT, Griffith JD, Kaguni LS. Structural rearrangements in the mitochondrial genome of Drosophila melanogaster induced by elevated levels of the replicative DNA helicase. Nucleic Acids Res [Internet]. 2018;46(6):3034–46. Available from: https://academic.oup.com/nar/advance-article/doi/10.1093/nar/gky094/4844048
120. Sedman T, Jõers P, Kuusk S, Sedman J. Helicase Hmi1 stimulates the synthesis of concatemeric mitochondrial DNA molecules in yeast Saccharomyces cerevisiae. Curr Genet [Internet]. 2005 Apr;47(4):213–22. Available from: http://www.ncbi.nlm.nih.gov/pubmed/15690159
121. Hug N, Longman D, Cáceres JF. Mechanism and regulation of the nonsense-mediated decay pathway. Nucleic Acids Research. 2015.
122. Khan NA, Auranen M, Paetau I, Pirinen E, Euro L, Forsström S, et al. Effective treatment of mitochondrial myopathy by nicotinamide riboside, a vitamin B3. EMBO Mol Med [Internet]. 2014 Jun;6(6):721–31. Available from: http://www.ncbi.nlm.nih.gov/pubmed/24711540
123. Tyynismaa H, Suomalainen A. Mouse models of {mtDNA} replication diseases. Methods. 2010;51(4):405–10.
124. Khan NA, Nikkanen J, Yatsuga S, Jackson C, Wang L, Pradhan S, et al. mTORC1 Regulates Mitochondrial Integrated Stress Response and Mitochondrial Myopathy Progression. Cell Metab [Internet]. 2017 Aug 1;26(2):419–428.e5. Available from: http://www.ncbi.nlm.nih.gov/pubmed/28768179
125. Carta A, D'Adda T, Carrara F, Zeviani M. Ultrastructural analysis of extraocular muscle in chronic progressive external ophthalmoplegia. Arch Ophthalmol (Chicago, Ill 1960) [Internet]. 2000 Oct;118(10):1441–5. Available from:

http://www.ncbi.nlm.nih.gov/pubmed/11030833
126. Gerhold JM, Cansiz-Arda S, Lohmus M, Engberg O, Reyes A, Van Rennes H, et al. Human Mitochondrial DNA-Protein Complexes Attach to a Cholesterol-Rich Membrane Structure. Sci Rep [Internet]. 2015;5:1–15. Available from: http://dx.doi.org/10.1038/srep15292
127. Rajala N, Gerhold JM, Martinsson P, Klymov A, Spelbrink JN. Replication factors transiently associate with mtDNA at the mitochondrial inner membrane to facilitate replication. 2014;42(2):952–67.
128. Cho B, Cho HM, Jo Y, Kim HD, Song M, Moon C, et al. Constriction of the mitochondrial inner compartment is a priming event for mitochondrial division. Nat Commun [Internet]. 2017;8:15754. Available from: http://www.nature.com/doifinder/10.1038/ncomms15754
129. Lewis SC, Uchiyama LF, Nunnari J. ER-mitochondria contacts couple mtDNA synthesis with Mitochondrial division in human cells. Science (80-). 2016;353(6296).
130. Jovaisaite V, Mouchiroud L, Auwerx J. The mitochondrial unfolded protein response, a conserved stress response pathway with implications in health and disease. J Exp Biol. 2014;217(1):137–43.
131. Tian Y, Merkwirth C, Dillin A. Mitochondrial {UPR:} A {Double-Edged} Sword. Trends Cell Biol. 2016;26(8):563–5.
132. Feng W, Yonezawa M, Ye J, Jenuwein T, Grummt I. PHF8 activates transcription of rRNA genes through H3K4me3 binding and H3K9me1/2 demethylation. Nat Struct Mol Biol. 2010;
133. Fortschegger K, de Graaf P, Outchkourov NS, van Schaik FMA, Timmers HTM, Shiekhattar R. PHF8 Targets Histone Methylation and RNA Polymerase II To Activate Transcription. Mol Cell Biol. 2010;
134. Kleine-Kohlbrecher D, Christensen J, Vandamme J, Abarrategui I, Bak M, Tommerup N, et al. A Functional Link between the Histone Demethylase PHF8 and the Transcription Factor ZNF711 in X-Linked Mental Retardation. Mol Cell. 2010;
135. Yu L, Wang Y, Huang S, Wang J, Deng Z, Zhang Q, et al. Structural insights into a novel histone demethylase PHF8. Cell Res. 2010;
136. Teperino R, Schoonjans K, Auwerx J. Histone methyl transferases and demethylases; Can they link metabolism and transcription? Cell Metabolism. 2010.
137. Suzuki A, Stern SA, Bozdagi O, Huntley GW, Walker RH, Magistretti PJ, et al. Astrocyte-neuron lactate transport is required for long-term memory formation. Cell. 2011;
138. Savtchouk I, Volterra A. Gliotransmission: Beyond Black-and-White. J Neurosci. 2018;
139. Felton CM, Johnson CM. Modulation of dopamine-dependent behaviors by the Caenorhabditis elegans Olig homolog HLH-17. J Neurosci Res. 2011;
140. Zarse K, Schmeisser S, Groth M, Priebe S, Beuster G, Kuhlow D, et al. Impaired insulin/IGF1 signaling extends life span by promoting mitochondrial L-proline catabolism to induce a transient ROS signal. Cell Metab. 2012;
141. Allen NJ, Lyons DA. Glia as architects of central nervous system formation and function. Science [Internet]. 2018;362(6411):181–5. Available from: http://www.ncbi.nlm.nih.gov/pubmed/30309945
142. Logan M, Logan M. Glial contributions to neuronal health and disease: new insights from Drosophila. 2017;

143. Richmond JE, Davis WS, Jorgensen EM. Unc-13 is required for synaptic vesicle fusion in C. elegans. Nat Neurosci. 1999;